The Electro-chemical Purification of Hydrogen using Polymer Electrolyte Membrane Fuel Cells

Ahmed Yusuf Abdulla

Submitted in Partial Fulfillment of the
Requirements for the Degree of Bachelor
of Science in Engineering

Advisor:

Professor Jay B. Benziger

Department of Chemical Engineering

Princeton University

May 2009

This paper represents my own work in accordance with University regulations.

I authorize Princeton University to lend this thesis to other institutions or individuals for the purpose of scholarly research.

Ahmed Yusuf Abdulla

I further authorize Princeton University to reproduce this thesis by photocopying or by other means, in total or in part, at the request of other institutions or individuals for the purpose of scholarly research.

Ahmed Yusuf Abdulla

Princeton University requires the signatures of all persons using or photocopying this thesis. Please sign below, and give address and date.

To Ahmed Abdulrahim and Mariam Juma.

You left your children and grandchildren far too soon, and showed nothing but love and kindness to everyone who has ever known you.

Acknowledgments

I am immensely appreciative of the guidance and support I have received from Professor Jay Benziger not only during the brief spell I spent in his lab, but also throughout my undergraduate career at Princeton. He has offered invaluable advice in his capacities as departmental representative and professor, and continues to do so as both an academic advisor and a mentor, and for that I am grateful.

I would also like to thank the graduate students in the Benziger Lab for their sound advice and continuous support: Erin Kimball, Josh Zhao, and May Jean Cheah. I would especially like to thank May Jean, without whose daily support, perseverance, and patience this project would have floundered.

The Alder Fund deserves special recognition for its support of senior theses projects, and so does the Crown Prince of Bahrain's International Scholarship Program whose generous support is responsible for my being at Princeton.

Most importantly, I shall remain forever grateful to my family. Despite being over 6,000 miles away, they have provided nothing but unconditional support throughout these four years. It is my mother, my father, and my brothers Fawaz and Feras who stood firmly beside me through thick and thin, and got me to where I am today. I thank them from the bottom of my heart.

Abstract

It has been proposed that Polymer Electrolyte Membrane (PEM) fuel cells be used as electrochemical (or hydrogen) pumps. Unlike standard fuel cells, which generate electricity from the chemical energy released when H_2 and O_2 combine to form water, electrochemical pumps require power – in the form of electricity – to pump hydrogen molecules from the anodic to the cathodic compartments of a cell by transporting them across the PEM. Since the PEM only allows for the transport of H_2 molecules, electrochemical pumps can theoretically be used to separate hydrogen from streams containing impurities, as one would find in the case of steam reforming, where both CO and CO_2 are present in large volumes along with the valuable hydrogen gas.

In this investigation, the performance of an electrochemical cell is analyzed at different currents, different temperatures, and different feed compositions. Pure hydrogen is fed into the cell at the anode, and pure nitrogen at the cathode. The performance of the pump at two temperatures, 54°C and 74°C, is investigated. At both temperatures, two currents of 0.5A and 1.0A are applied to the cell. Our analysis suggests that temperature has virtually no effect on the cell's power requirement or the cell's efficiency.

A mixed stream of 3:1 H_2:CO_2 is then introduced to the cell. Our runs show that temperature has no effect on the cell's efficiency or the separation efficiency. CO_2 concentration at the cathode was less than 200ppm in all cases, indicating high separation efficiency. However, we notice some degradation in performance at both temperatures. There is some evidence to suggest that performance degradation increases at higher temperatures thanks to the formation of CO through the reverse water gas shift (RWGS)

reaction. As expected, current is the only factor that determines the hydrogen yield at the cathode.

The H_2 flow is then reduced – and the CO_2 flow rate held constant – in order to investigate the effect of feed composition on fuel cell performance. Results indicate that, as the concentration of H_2 in the feed decreases, more power is required to drive the H_2 molecules across the membrane. The increase in power requirement appears to be exponential in relation to H_2 volume fraction in the feed. Moreover, as the concentration of H_2 in the feed decreases, fuel cell performance becomes more erratic. Since this phenomenon appears to be reversible without the introduction of current pulsing or an air bleed, it is most likely that the dilution of H_2 in the feed is the cause of this erratic behavior, and of the increase in power requirement as opposed to CO poisoning. Hydrogen yield, however, remains unaffected. Also, as the concentration of CO_2 in the feed increases, more CO_2 diffuses to the cathodic compartment and into the product stream, lowering the separation efficiency.

Simulations of 4-cell and 6-cell electrochemical pumps are performed: the former has a H_2 yield of 67%, while the latter's H_2 yield is virtually 100%. This high yield comes at the expense of both higher potentials (and, thus, higher power requirements) and lower separation efficiencies (99.85% for the 4-cell pump as opposed to 99.72% for the 6-cell pump). Both simulations suggest that the use of low-power, low-temperature PEM cells as hydrogen pumps is a viable alternative to the high-cost, high-power separation techniques employed today such as pressure swing adsorption and cryogenic distillation, especially when it comes to localized (or regional) settings or to remote applications.

Table of Contents

		Page
Part I – Introduction		1
Part II – Background Information		
i.	The Looming Energy Crisis	3
ii.	An Introduction to PEM Fuel Cells	4
iii.	Hydrogen Production and Purification Techniques	7
iv.	Hydrogen Pumps in Literature	11
Part III – Materials and Methods		
i.	The Workings of a Hydrogen Pump	14
ii.	Building a Differential PEM Fuel Cell	20
iii.	Describing the Experimental Setup	22
iv.	Data Acquisition Techniques	24
Part IV – Results and Discussion		
i.	The Effect of Temperature on Hydrogen Pumping	25
ii.	A Simulation of a Stack of PEM Differential Elements	39
iii.	An Investigation into H_2 Pumping's Economic Feasibility	44
Part V – A Discussion of Experimental Limitations		49
Part VI – Conclusions		50
Part VII – Future Work		51

List of Figures

Figure 1	The Growing Gap: Oil Production vs. Oil Discovery	3
Figure 2	PEM Fuel Cell Operating in Standard Mode	5
Figure 3	PEM Fuel Cell Operating in Hydrogen Pumping Mode	14
Figure 4	The STR PEM Fuel Cell Electrode Design	21
Figure 5	Exploded View of Assembled STR PEM Fuel Cell	21
Figure 6	A Schematic of the Experimental Setup	23
Figure 7	Pure H_2: I and V vs. t at FC temperature of 54°C	26
Figure 8	P_{thermo} vs. P_{ion} and P_{OPL} for both 54°C Control Runs	28
Figure 9	Ohmic losses: R_{int} vs. R_{avg} at different current holds	29
Figure 10	Pure H_2: I and V vs. t at FC temperature of 74°C	31
Figure 11	P_{thermo} vs. P_{ion} and P_{OPL} for both 74°C Control Runs	32
Figure 12	3:1 H_2:CO_2: I and V vs. t at FC temperature of 54°C	33
Figure 13	P_{thermo} vs. P_{ion} and P_{OPL} for both 54°C 3:1 H_2:CO_2 Runs	35
Figure 14	A Representation of Cell Operation at 3:1 H_2:CO_2	35
Figure 15	3:1 H_2:CO_2: I and V vs. t at FC temperature of 74°C	36
Figure 16	P_{thermo} vs. P_{ion} and P_{OPL} for both 74°C 3:1 H_2:CO_2 Runs	37
Figure 17	A Comparison of Cell Operation with and without CO_2	39
Figure 18	Representation of a Stack of Electrochemical H_2 Pumps	40
Figure 19	V vs. t for a 4-cell stack simulation	40
Figure 20	Power required in each cell of a 4-cell H_2 Pump	41
Figure 21	V vs. t for a 6-cell stack simulation	42
Figure 22	Power required in each cell of a 6-cell H_2 Pump	42
Figure 23	H_2 yield vs. separation efficiency in a 6-cell stack	44
Figure 24	Energy Requirements and Costs Associated with High H_2 Yield	46
Figure 25	Change in Power vs. Change in Yield in a 6-cell Stack	47
Figure 26	Energy Input into Cell vs. Energy Content of H_2 Output	49

List of Tables

Table 1	V_{avg} and P_{av} for the control runs at 54°C	27
Table 2	V_{avg} and P_{av} for the control runs at 74°C	31
Table 3	Potential Variation, V_{avg}, and P_{av} for the 54°C 3:1 H_2:CO_2 Runs	33
Table 4	Potential Variation, V_{avg}, and P_{av} for the 74°C 3:1 H_2:CO_2 Runs	37

Part I – Introduction

One of the pressing issues facing the world today is the expected depletion of fossil fuel reserves, and the challenges that situation would create for the world economy, particularly for the transportation sector which relies almost exclusively on liquid hydrocarbon fuels derived from crude oil [1]. Of the alternative energy sources proposed for the transportation sector, none has gained as much traction (or publicity) as hydrogen. The U.S. government has committed itself to supporting many technologies that could substitute for internal combustion vehicles, including the development of a hydrogen infrastructure. Several international and U.S. agencies (primarily the Departments of Transportation and Energy, DOT and DOE, respectively) have been working actively with researchers and academia to better understand and overcome the challenges facing the institutionalization and commercialization of hydrogen technologies [2,3,4]. The ultimate aim of the hydrogen infrastructure is to feed fuel cell vehicles (FCVs) which – instead of burning fossil fuels to generate the kinetic energy of motion – would combine hydrogen and oxygen (the latter from the air) to produce electricity and water: the former can be used to drive an electric motor, while the latter can be harmlessly exhausted into the atmosphere.

Molecular hydrogen is not found naturally on Earth: it needs to be produced. Despite recent research into reverse fuel cell operation and electrolysis using nuclear power, steam reforming of natural gas remains the most widely used method of producing hydrogen on an industrial scale. It accounts for over 95% of hydrogen produced in the U.S. and almost half of all hydrogen produced worldwide [5].

The production of hydrogen through steam reforming generates carbon monoxide (CO), carbon dioxide (CO_2), and water vapor (H_2O) as byproducts. While the removal of water vapor is a trivial operation, the separation of the gaseous compounds from the hydrogen is a more delicate task that is made very important by the fact that carbon monoxide and carbon dioxide impair the performance of the polymer electrolyte membrane (PEM) fuel cells that would power FCVs. CO poisons the platinum catalysts used in PEM fuel cells, and CO_2 can both block adsorption sites on the fuel cell membrane or be chemically reduced to CO, which would again poison the catalyst. It is therefore crucial to remove these contaminants from the reformate before introducing it to a PEM fuel cell.

This paper investigates a method of removing the vast quantity of CO_2 from reformate streams. A fuel cell is operated at low currents as a hydrogen pump whereby a mixed stream of H_2 and CO_2 is introduced to the cell at the anode inlet, and a nitrogen stream is introduced at the cathode inlet. When a current is applied to the cell, the chemical potential difference of hydrogen between the anode and cathode generates a voltage. H_2 from the anode is pumped across the membrane to the cathode, yielding H_2 of a very high purity at the cathode outlet: this H_2 can then be used in PEM fuel cells. This setup is tested at various gas compositions and various temperatures. Experiments that simulate hydrogen pumping fuel cell stacks are also carried out.

Part II – Background Information

i. The Looming Energy Crisis:

According to the International Energy Agency, the remaining proven reserves of oil and natural gas are large enough to sustain human activity over the next forty years [6]. This conclusion derives from a reference case that incorporates estimated increases in oil production, but assumes no growth in demand for oil beyond averaged 2008 figures [6]. However, the level of annual global oil production has consistently outstripped the level of annual discoveries for more than two decades, as figure 1 demonstrates. Furthermore, the level of discoveries is projected to exponentially decrease.

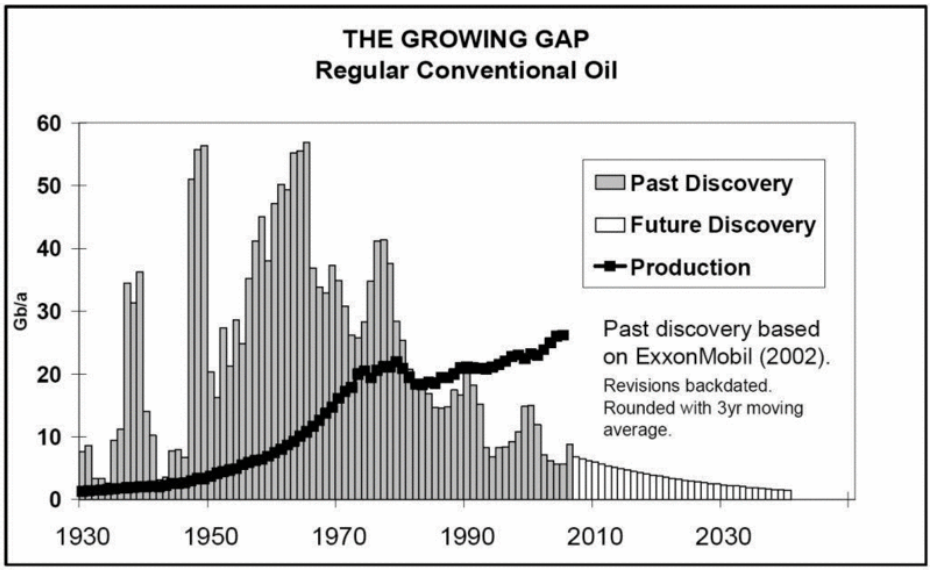

Figure 1: *Annual oil production has been greater than annual discoveries since the early 1980s. The gap is only expected to grow as projections show an exponential decline in future discoveries [7].*

Despite the 2008-2009 recession and the associated crash in oil prices, the major economies of the developing world (mainly Brazil, India, and China) are expected to grow at considerable rates in the coming years [8,9]. As these economies grow, they will witness a transportation revolution: India's transport energy demand is expected to grow

fourfold by 2030, and Chinese vehicle sales are expected to overtake those of the U.S. within the next five years [10]. Nearly 70% of the 20.7 million barrels of liquid fuel consumed in the United States every day is dedicated to the transportation sector [11], and liquid fuels service more than 95% of the global transportation infrastructure [10]. Shell estimates that demand for oil and natural gas products will finally begin to outstrip supply by 2015 [12].

Fossil fuel reserves will thus be exhausted in the coming decades and, considering the growth expected in energy demand, it is imperative that research into alternative energy sources continues unabated. One technology that can alleviate some of the world's energy concerns is the fuel cell, which converts chemical energy into electrical energy. Several types of fuel cells exist, but the one that is most suited for mobile applications (such as FCVs) is the PEM fuel cell, where hydrogen and oxygen react to form water, generating energy in the process.

ii. An Introduction to PEM Fuel Cells:

PEM fuel cells are electrochemical power sources that convert the chemical energy released when hydrogen and oxygen combine to form water into electrical energy. Fuel cells are thus very similar to batteries but, while batteries are closed systems that have a fixed amount of reactants that chemically combine to release energy, fuel cells are open systems where reactants may be fed continuously. Figure 2 shows a profile of a PEM fuel cell.

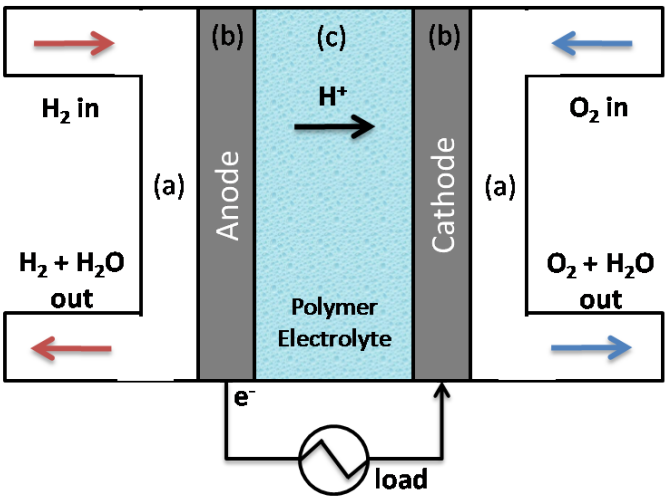

Figure 2: *A PEM fuel cell operating in standard mode. Hydrogen and oxygen are fed at the anode and cathode, respectively. The hydrogen molecule dissociates into protons and electrons. The protons are pumped across the membrane, while their electrons are transmitted through an external circuit.*

There are five major components to a PEM fuel cell as figure 2 illustrates: the first two – represented by (a) in the figure above – are the gas flow channel complexes that are necessary to transport the gas molecules at either anode or cathode to the electrode interface in both compartments. The second two components – represented above by (b) – are the two electrodes, the anode and the cathode, whose job is to transfer electrons either to, or from, the chemical species reacting at their interface. The electrodes can be made of any conducting material – the layer that catalyzes the dissociation of gases at the three-way interface of gas, catalyst, and electrolyte membrane is part of the electrode (the catalyst at both anode and cathode is platinum supported on carbon or Pt/C).

The final component (c) is the electrolyte membrane itself which permits the transmission of electrons from one compartment to another (and hence, of electric current to an external load). The most commonly used membrane is Nafion®, originally produced by DuPont. Nafion® is a sulfonic acid ionomer which serves as a conductor of protons.

An ideal PEM would not conduct any electrons across the membrane, would not permit the crossover of gases from the anodic compartment to the cathodic compartment (or vice versa), and would resist the harsh environments at either compartment (the oxidizing environment at the anode and the reducing environment at the cathode). However, this membrane must be nearly fully humidified to minimize its internal resistance, allowing it to operate at optimum capacity [13]. The membrane is sandwiched between the two electrodes to construct a 'membrane electrode assembly' or MEA.

At the anode, hydrogen gas dissociates into protons and electrons. The former is transported across the electrolyte membrane to the cathode, while the latter is transported to the cathode terminal through an external circuit that passes through an external load. Reaction (1) below highlights the oxidation reaction that occurs at the anode:

$$H_2 \rightarrow 2H^+ + 2e^- \quad (1)$$

At the cathode, the hydrogen ions that were transported from the anode combine with oxygen and the unbroken circuit's electrons to form water in the following reaction:

$$O_2 + 4H^+ + 4e^- \rightarrow 2H_2O \quad (2)$$

PEM fuel cells are especially suited to both remote and mobile applications such as FCVs because of their low temperature operation and compactness. This compactness means that they also lend themselves well to a modular design. The main disadvantages associated with PEM fuel cells are: (1) the expense associated with MEA production (both the Nafion® membrane and the catalyst layer are expensive), (2) the complex issue of water management (an excess of water results in flooding which blocks the three-way interface of gas, catalyst, and PEM [13], while a deficit of water dries out the membrane;

both conditions harm the fuel cell's power output), and (3) the issue of catalyst poisoning. The main PEM fuel cell poison is CO which, when present even at low concentrations [14], competes with H_2 for adsorption on catalyst sites, thus reducing the cell's power output [15]. An excess of CO_2 is also harmful because it blocks H_2 access to adsorption sites on the membrane; also, if CO_2 is reduced to CO inside the fuel cell, it will poison the cell as described earlier. It is therefore essential that hydrogen fed into a PEM fuel cell be free of contaminants including both CO and CO_2.

iii. Hydrogen Production and Purification Techniques:

As mentioned in the introduction, steam reforming of natural gas is the primary method of producing hydrogen at a scale large enough to satisfy industrial demand [5]. Other methods of hydrogen generation have been proposed; these include the electrolysis of liquid water and water photolysis. Electrolysis is an energy intensive process (the electrolysis of one mole of water yields one mole of hydrogen and requires at least 282.1 kJ of energy) [16] that would require dedicated energy providers to function on a large scale (such as nuclear power stations). Water photolysis – the use of solar hydrogen cells to split water into its gaseous constituents – is a relatively new technology whose laboratory efficiency currently stands at 0.3% [17]. Once these technologies are studied extensively in laboratories and commercialized, it is foreseeable that the efficiency of solar hydrogen cells will increase to between 10 and 15% [17]. Nevertheless – at least in the interim – steam reforming will remain the workhorse method for hydrogen generation, and its importance as a near-term method of hydrogen production has been established [18].

Steam reforming involves the production of hydrogen from fossil fuel sources, mainly from methane, but other light hydrocarbons may be used as well. Reactions (3) to (7) below illustrate how light hydrocarbons react catalytically with high temperature steam (700°C to 1000°C) to produce hydrogen and carbon monoxide [18].

Methane: $$CH_4 + H_2O \rightarrow CO + 3H_2 \quad (3)$$

Propane: $$C_3H_8 + 3/2\,O_2 \rightarrow 3CO + 4H_2 + \Delta \quad (4)$$

Ethanol: $$C_2H_5OH + 1/2\,O_2 \rightarrow 2CO + 3H_2 + \Delta \quad (5)$$

Iso-octane: $$C_8H_{18} + 4O_2 \rightarrow 8CO + 9H_2 + \Delta \quad (6)$$

Toluene: $$C_7H_8 + 7/2\,O_2 \rightarrow 7CO + 4H_2 + \Delta \quad (7)$$

America's most abundant fossil fuel, coal [34], can be gasified to form synthesis gas, as reaction (8) illustrates, in a process that is used widely to generate electricity:

Coal gasification: $$Coal + O_2 + H_2O \rightarrow CO + H_2\ (unbalanced) \quad (8)$$

The DOE's 'Hydrogen from Coal Multi-Year R&D Plan' presents – in detail – the expected improvements in gasification technology that will make this route a commercially viable option for hydrogen production in the future [34]. Environmental viability, however, is a major cause for concern. Due to the large amounts of CO_2 that are produced in this process, adopting it on a large scale will require carbon capture and storage. Recognizing this fact, the DOE is running a carbon sequestration R&D initiative parallel to the 'Hydrogen from Coal' program. The ideal sequestration technologies should prove effective, cost-competitive, stable, and environmentally benign [29]. Current sequestration methods cost between $100 and $300 per ton of carbon emissions

avoided, and the goal is to reduce these costs to under $10 per ton [29], so there is a long way to go before carbon sequestration can be adopted on a large scale.

The synthesis gas (syngas) resulting from these reactions is then fed into a water gas shift reactor, where CO reacts with H_2O to form CO_2 and H_2. This step is important for two reasons: first, it increases the hydrogen yield from the entire operation and, second, it reduces the amount of CO the refinery must deal with. CO is poisonous and its release into the atmosphere is strictly avoided. Instead, CO is usually oxidized to CO_2 at the final stages of the operation and exhausted into the atmosphere. Given this information, the most likely syngas composition that electrochemical hydrogen pumps will be required to purify can be represented by the following equations:

Reforming: $$CH_4 + H_2O \rightarrow CO + 3H_2 \quad (9)$$

Water gas shift: $$CO + H_2O \leftrightarrow CO_2 + H_2 \quad (10)$$

If all the CO is oxidized to CO_2 before it is fed into the fuel cell, this would mean that the ratio of H_2:CO_2 would be 3:1 after the reforming reaction (9). If all the CO is sent to a water gas shift reactor as opposed to a catalytic oxidizer as it would be after the combination of reactions (9) and (10) is carried out, then the resulting ratio of H_2:CO_2 would be 4:1.

As emphasized in the previous section, CO poisons the membrane in a PEM fuel cell. It is therefore imperative that the CO concentration in the reformate be reduced to negligible levels (very low ppm). There are several methods of isolating the hydrogen in the reformate to a very high purity. Perhaps the method most widely used in industry is pressure swing adsorption (PSA), where the reformate is pumped through a drum containing fixed-bed adsorbents at high pressure. These adsorbents (usually molecular

sieves) are configured to increase the affinity of impurities like CO and CO_2 to the adsorbent material. Hence, while the hydrogen escapes to the top of the drum, the impurities are adsorbed in the drum. As soon as the sieves reach their full adsorption capacity, a valve prevents their release into the pure hydrogen stream, and depressurization regenerates the adsorbents, and the desorbed gases are purged from the drum [19]. PSA's disadvantages include its high capital cost and its complexity: multiple drums are needed for continuous operation. Also, while hydrogen purity is very high, some hydrogen is lost when the vent valves are closed and the drum contents are purged.

Other methods of purifying hydrogen include cryogenic distillation and various membrane separation techniques. The former method is most commonly used to separate atmospheric nitrogen from other components in air (primarily so that it can be used in the Haber process). Cryogenic distillation involves the separation of the different components of the reformate at temperatures of -185°C [20]. It is therefore very expensive and – like PSA – it does not lend itself to localized or remote applications: these units need to be part of a refinery, and are only suitable for large-scale hydrogen generation plants as opposed to the distributed (regional or sub-regional) plants that would reduce costs associated with hydrogen transportation and delivery. Several adsorbents – including molecular sieves – have been proposed for use in the petroleum industry to remove contaminants like CO_2 from gaseous streams [21]. Other types of membrane separators include palladium and micro-porous silica materials [14]. Much like the other processes discussed, membrane separation would be far too costly a technique to implement in homes and cities without a simplification of the apparatus.

Given the limitations in current separation techniques and the high cost associated with separation processes of this nature [14], it is thus useful to explore other methods of hydrogen purification that can be implemented easily on local and regional levels [22], such as the use of PEM fuel cells as electrochemical pumps, transporting the reformate's hydrogen from the anodic to the cathodic compartment of the fuel cell.

iv. Hydrogen Pumps in Literature:

There are several applications for hydrogen pumping using PEM fuel cells. The use of such cells as electrochemical hydrogen compressors has been studied [23], where the large pressure difference between the anodic and cathodic compartments allows for pumping from one side to the other with high process efficiency, high purification capacity, and low power requirements. More recently, PEM fuel cells have been combined with electrochemical pumps (also PEM fuel cells) for the purpose of hydrogen recirculation in fuel cell stacks [24]. The third major application is their use as stream purifiers or as hydrogen separators.

The idea of using PEM fuel cells as hydrogen pumps for the purpose of purification of mixed streams was pioneered in the 1980s by Sedlak et al [25]. However, the amount of literature dedicated to the subject is limited, and the idea has only recently been revived. Engineers and chemists have long since recognized the negative effect of CO's presence – even in low ppm quantities – on fuel cell performance, and have thus opted to focus on improving catalyst operation at a wide range of conditions [26], as well as on re-engineering PEMs to increase their resistance to CO poisoning [14, 26].

Recently, Perry et al. [14] analyzed the performance of PEM fuel cells as hydrogen pumps while operating the cell at high temperatures with a PA-doped polybenzimidazole (PBI) membrane. The group experimented with multiple gas mixtures, including pure hydrogen, premixed natural gas reformate (35.8% H_2, 1906 ppm CO, 11.9% CO_2, and N_2 balance), and premixed methanol reformate (69.17% H_2, 1.03% CO, and 29.8% CO_2). The feeds were humidified through an external tank which maintained 3% relative humidity at 160°C – it is at this high temperature that most of their runs were performed. They noted that the pump required low power while achieving excellent durability with little degradation in fuel cell performance during long-term tests. Gardner and Ternan [15] also studied the electrochemical separation of hydrogen from a reformate stream with 1000 ppm CO. Their setup used a standard Nafion® 115 membrane with carbon supported Pt and Ru at both electrodes. Their cell's flow channel appears to be of the serpentine variety, and constant humidification of the cathode is required. They determined that the efficiency of hydrogen pumping was highest with pure hydrogen (as expected), but that the efficiency of separation was low. Indeed, CO severely poisoned their anode catalyst and raised their potential considerably. To minimize CO's poisoning effect, they suggest that periodic pulses of current be applied.

Casati et al. [27] attempted to expand the literature by experimenting with hydrogen purification and hydrogen compression at multiple conditions. The group used a mixture of H_2 and N_2, and experimented with hydrogen pump operation at both galvanostatic and tensiostatic conditions. Their runs suggest that operation at galvanostatic conditions is inherently unstable, whereas setting the driving force and measuring the rate of hydrogen recovery (tensiostatic conditions) produced stable results.

They also tried to examine the role of water in hydrogen pump mode as opposed to fuel cell mode, as well as the cell efficiency as a function of hydrogen yield; they claim that, as the cell voltage increases, the cell efficiency increases correspondingly. There is not enough data, however, to firmly establish the precise nature of the empirical trend. It is noteworthy that Casati et al. use two different cells – these have different flow channel configurations. The first one of these has 21 separate parallel flow channels, while the second is serpentine: it is composed of a single long zigzag channel. In both cases, the MEA is of identical size. However, the serpentine cell's channel volume of 5.28 cm^2 is 90% greater than that of the cell with parallel channels, whose volume stands at 2.88 cm^2. While they conclude that the shape of the distribution channels has no influence on the process, the effect of the mixtures on current distribution is only fleetingly discussed.

Tingelöf et al. [28] studied the effects of CO_2, CO, and air bleed on the current distribution of a PEM fuel cell. The group presents a discussion of how CO_2, CO, and air bleed influence fuel cell operation, introducing most of the theories put forth by researchers thus far. They conclude that, while CO_2 does not greatly influence current distribution, it does have a negative effect on the PEM fuel cell's voltage. They suggest that the perceived 'dilution' of the hydrogen in the inlet stream (as a result of the presence of CO_2, a problem that has been suggested in part II, section ii of this paper) plays a role in increasing the potential required for hydrogen pumping. The effect – they suggest – is catalytic, meaning that any poisoning of the catalyst layer at the anode caused by the CO_2 can be counteracted with air bleed, a method that has been proved beneficial for CO poisoning by their group, but also by Garnder and Terner (2007). As expected, the influence of CO poisoning is far more severe. CO poisoning causes

significant changes to the distribution of current in the fuel cell, according to Tingelöf et al. This is especially true when the catalyst used is Pt/C as opposed to PtRu/C, the latter being more resistant to the effects of such poisoning. An analysis of the dynamic response of the fuel cell to CO poisoning shows that the effect of the poisoning takes hold slowly – the group suggests that an impulse of the poisons would not seriously poison the catalyst. As expected, given their in-depth analysis of current distribution, the fuel cell they employ is serpentine and segmented in nature, allowing for analysis of current distribution at various points downstream of the gas inlet ports.

Part III – Materials and Methods

i. The Workings of a Hydrogen Pump:

The operation of a PEM fuel cell as an electrochemical hydrogen pump differs from that of a regular PEM fuel cell as described in part II, section ii of this paper. Figure 3 shows a PEM fuel cell operating as an electrochemical hydrogen pump:

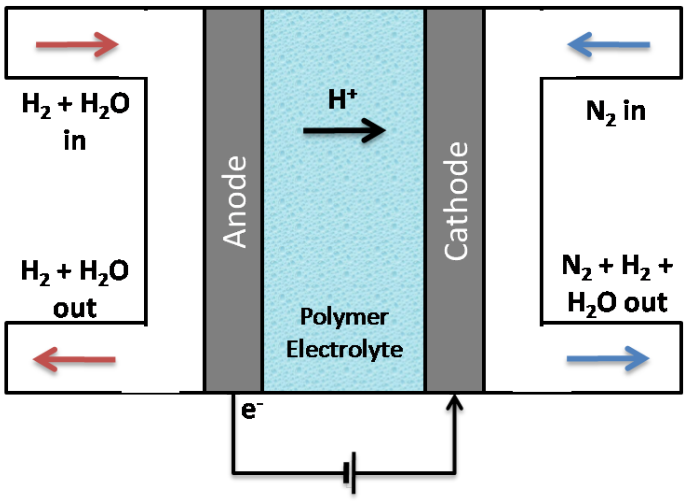

Figure 3: *Representation of a PEM fuel cell operating in hydrogen pumping mode. A humidified feed of hydrogen is fed to the fuel cell at the anode (along with any impurities it may contain). Dry nitrogen is fed at the cathode. The hydrogen molecule dissociates into protons and electrons. The protons are pumped across the membrane, while their electrons are transmitted through an external circuit.*

Unlike standard fuel cell operation, the feed to a hydrogen pump is composed of a hydrogen gas stream (along with any impurities that stream may contain) at the anode and a nitrogen gas stream at the cathode. The purpose of the nitrogen is to act as a vehicle for water and hydrogen gas removal from the cathodic compartment. It is not necessary for hydrogen pump operation; the pump may function with the inlet to the cathode sealed. The feed must be humidified – near total humidification is necessary for the Nafion® PEM's operation. A power source is needed to supply power to the PEM fuel cell for hydrogen pumping to occur. The power supply also completes the external circuit that is necessary for electron transport from anode to cathode upon the dissociation of hydrogen molecules at the anode.

When a voltage is imposed on the cell, the hydrogen atoms adsorbed at the anode surface are split into protons and electrons as illustrated by reaction (1). The electrons pass through the external circuit on their way to the cell's cathode compartment, while the protons are transported across the membrane to the cathode. At the cathode, the protons and electrons combine to reconstitute hydrogen molecules. Water is also transported through diffusion across the membrane (this is a result of the presence of a concentration gradient), or through electro-osmotic drag [30]. A dry nitrogen stream is fed at the cathode in order to draw out the hydrogen and water molecules at the cathode interface from the cell compartment.

The purification of hydrogen using electrochemical pumping is a novel method because it does not rely – like other purification techniques – on pressure differentials or extreme temperature conditions. Rather, it is wholly dependent on applied current, as dictated by Faraday's Law of electrolysis:

$$I = z\mathfrak{F}\frac{\mathrm{d}n}{\mathrm{d}t} \tag{11}$$

where I is the applied current, z is the number of (valence) electrons – 2 in the case of hydrogen – and $\mathfrak{F}$ is Faraday's constant. The voltage (potential) required for hydrogen pumping can also be determined using the Nernst equation:

$$V_{thermodynamic} = \frac{\mathrm{RT}}{z\mathfrak{F}}\ln\left(\frac{\mathrm{P}_{\mathrm{H}_2}^{\mathrm{cathode}}}{\mathrm{P}_{\mathrm{H}_2}^{\mathrm{anode}}}\right) \tag{12}$$

where R is the ideal gas constant, T is the absolute temperature, and $\mathrm{P}_{\mathrm{H}_2}^{\mathrm{c}}/\mathrm{P}_{\mathrm{H}_2}^{\mathrm{a}}$ is the pressure ratio across the PEM (a ratio of hydrogen activity at the cathode to hydrogen activity at the anode). At constant current, applied over a period of time, equation (11) becomes:

$$\dot{n} = \frac{MI}{z\mathfrak{F}} \tag{13}$$

where M is the gas's molar mass and $\dot{n}$ is the mass flow rate in gs^{-1}.

When a PEM fuel cell operates in hydrogen pumping mode, the power supply should impose as negligible a load as possible. However, the membrane has a resistance, which is referred to as the cell's internal resistance, R_{int}. The relationship between the cell's potential and the applied current can therefore be deduced from Ohm's Law:

$$I = \frac{V_{thermodynamic}}{R_{int}} \tag{14}$$

The power required for this hydrogen pumping operation can thus be calculated: it is the product of applied current and voltage:

$$P = IV_{thermodynamic} \quad (15)$$

The thermodynamic voltage, $V_{thermodynamic}$, is always smaller than the actual voltage that will be measured when operating the cell in hydrogen pumping mode. This is mainly due to losses such as ohmic resistance; these losses serve to increase the driving force (potential) required for the hydrogen pumping operation. This discrepancy between the Nernst voltage ($V_{thermodynamic}$) and the recorded voltage must be taken into account and, in commercial applications, minimized as much as possible.

If impurities are present in the anode feed stream, they will not be transported across the Nafion® membrane. The only possible mechanism for CO or CO_2 transport from the anodic to the cathodic compartment is diffusion. The vast majority of gaseous impurities should exit the cell from the anode's outlet – along with water and any hydrogen that was not pumped across the membrane.

These impurities would be in the form of the CO and CO_2 present after steam reforming and WGS. Exactly how much CO and CO_2 exist in the reformate once the reforming and shift reactions are complete depends on many factors, including catalyst choice, temperature, feed ratio, and reactor space velocity. Reactions (9) and (10) will be reproduced here as reactions (16) and (17) to facilitate discussion of this process:

Reforming: $$CH_4 + H_2O \rightarrow CO + 3H_2 \quad (16)$$

Water gas shift: $$CO + H_2O \leftrightarrow CO_2 + H_2 \quad (17)$$

The WGS reaction is most often performed using a $Cu/ZnO/Al_2O_3$ catalyst [37]. The equilibrium constant K_{eq} is given by the following two equations [37]:

$$K_{eq} \cong \frac{P_{CO_2} P_{H_2}}{P_{H_2O} P_{CO}} \quad (18)$$

$$K_{eq} = \exp\left(\frac{4577.8}{T} - 4.33\right) \quad (19)$$

The equilibrium constant can be calculated from (19) at different temperatures. At 200°C, it is 210, and it decreases as temperature increases because the WGS reaction is relatively exothermic ($\Delta H_{298}^{O} = -41.1 kJ/mol$). After the reforming operation is complete, the WGS feed is composed of 1:1 H_2O:CO. Choi and Stenger's (2003) experimental results can be adapted to the conditions we desire which would suggest that, at 200°C and a 1:1 H_2O:CO ratio, the CO exiting concentration for equilibrium conversion will be 30,000 ppm (for an equilibrium conversion of roughly 75%). The CO concentration may be reduced to hundreds of ppm by increasing the H_2O:CO ratio to 2:1, 3:1, or perhaps 4:1 by injecting water into the system. At 4:1, for example, the equilibrium conversion at 200°C would be greater than 90% (roughly 10:1 CO_2:CO). Operating procedures would obviously be varied after detailed analysis should a WGS plant be dedicated to producing low CO reformate intended for fuel cell use.

A lot has been said about the influence of CO and CO_2 on PEM fuel cell performance. A discussion of the mechanisms by which these gases interact with the catalyst layer is thus in order. The mechanism by which CO poisons the Pt/C catalyst of PEM fuel cells has been established [15]. CO competes with hydrogen for adsorption onto the Pt catalyst sites at the anode, which increases anode operating potentials, since the driving force required for hydrogen pumping increases as the number of active catalyst sites decrease. Equations (20) and (21) illustrate how hydrogen catalytically dissociates at the catalyst layer, while equation (22) highlights the CO poisoning mechanism (competitive adsorption). Note that the S in the equations represents a Pt catalytic site on the anode:

$$H_2 + 2S \leftrightarrow 2H - S \quad (20)$$

$$2H - S \leftrightarrow 2S + 2H^+ + 2e^- \quad (21)$$

$$CO + S \leftrightarrow CO - S \quad (22)$$

This poisoning effect can be reversed by raising the anode's potential, which allows for the reaction of CO with hydroxyl groups (which form upon the dissociation of water at the Pt interface and occupy catalytic sites), forming CO_2.

$$H_2O + S \leftrightarrow S - OH + H^+ + e^- \quad (23)$$

$$CO - S + OH - S \rightarrow 2S + CO_2 + H^+ + e^- \quad (24)$$

The mechanism for the reactions that occur when CO_2 interacts with the anode catalyst layer is not as well-established as that for CO poisoning. What has been established both empirically and through simulations is the presence of CO on the anode catalyst layer after the injection of reformate streams into PEM fuel cells [28]. Tingelöf et al. (2008) presented the two most common theories behind this phenomenon: first, that the CO_2 and adsorbed hydrogen react to form the CO in a variant of the reverse water gas shift (RWGS) reaction [28, 31]; second, that the reaction is actually an electrochemical reduction from CO_2 to CO. Equation (25) highlights the mechanism behind the RWGS reaction that occurs in the cell, while equation (26) illustrates the electrochemical reduction reaction that has been proposed [28, 32]:

RWGS: $$CO_2 + 2Pt - H \leftrightarrow Pt - CO + H_2O + Pt \quad (25)$$

Reduction: $$CO_2 + 2H^+ + 2e^- + Pt \leftrightarrow Pt - CO + H_2O \quad (26)$$

This study of H_2 purification from mixed H_2 and CO_2 streams will focus on steady-state operation as opposed to the dynamics of electrochemical pumping. A PEM

fuel cell simulating one differential element will be used in the study. The operation of such differential PEM fuel cells, whose design will be explained in the following section, mimics that of coupled stirred tank reactors, allowing for a detailed analysis of steady-state operation.

ii. Building a Differential PEM Fuel Cell:

The PEM fuel cell used in this investigation was custom built and behaves as a coupled stirred tank reactor (STR). Its design has already been discussed in papers published by our group [13], but will be discussed below for thoroughness. The STR design replaces the gas flow channels seen in most commercial applications with an open plenum that allows for thorough gas mixing. The open plenum has four distributed pillars of equal height that apply uniform pressure on the MEA once the fuel cell's connecting bolts are tightened. Taking the surface area of the four pillars into consideration, the interface between the electrode and the electrolyte has a surface area of $1.9cm^2$. Injection and exhaust ports are drilled into each graphite electrode and, while the injection ports are parallel to the horizontal, those of the exhaust are angled for gravity-assisted drainage. Figure 4 illustrates the design of the STR, or differential, PEM fuel cell electrodes through both side and profile views. Two such electrodes were machined, one for the anodic compartment and one for the cathodic compartment. The MEA was comprised of two silicon gaskets, two carbon cloth E-TEK electrodes (DeNora, NJ, USA) whose PEM-facing layer contained the Pt/C catalyst, and the Nafion® 115 membrane (Ion Power Inc, DE, USA) which was activated by boiling in H_2O_2, DI, 1M H_2SO_4, and DI for

one hour per step. The MEA was hand-assembled and pressed, upon which it was ready for placement between the two graphite electrodes.

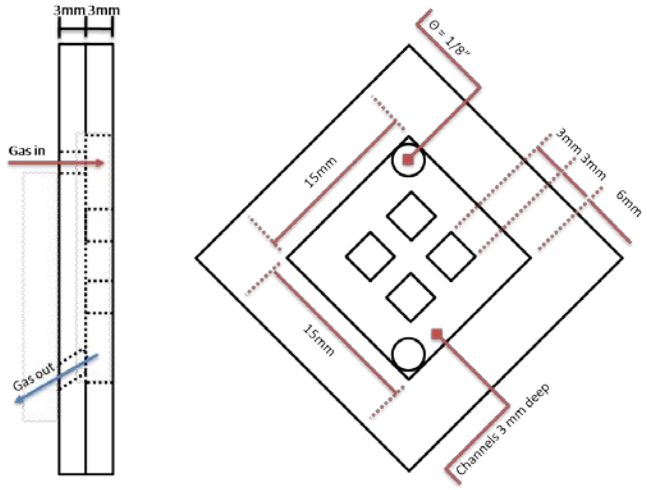

Figure 4: *Side (left) and profile (right) views of the STR PEM fuel cell electrodes. As explained above, they are channel-less and allow for gravity-assisted self-drainage.*

Once the MEA was sandwiched between the two electrodes, the setup was supported at both ends by Teflon plates, and this assembly was again supported by two stainless steel plates that acted as heat sinks to control temperature. This was accomplished by drilling cylindrical ports into the two stainless steel plates for the insertion of cartridge heaters whose operation was managed by a temperature controller. Figure 5 is an exploded 3D model of the assembled PEM fuel cell.

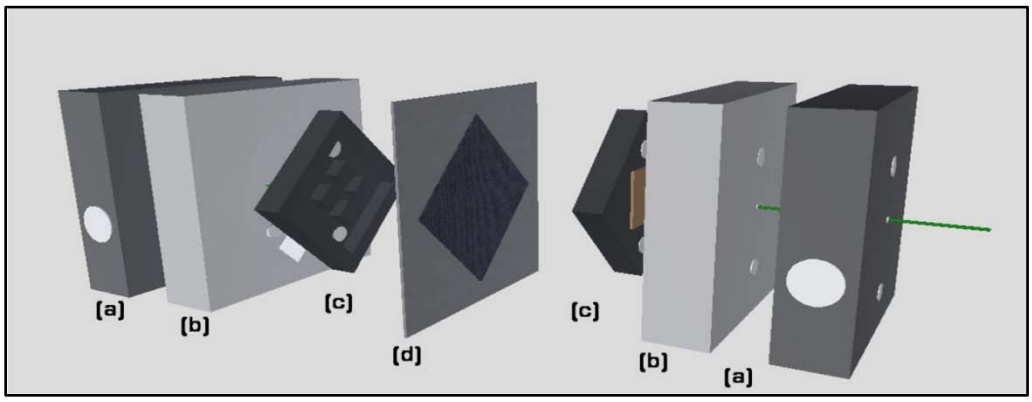

Figure 5: *An exploded view of the assembled PEM fuel cell. The MEA (d) is sandwiched between the two graphite channel-less self-draining electrodes (c). These are embedded into Teflon plates (b), which are supported by stainless steel heat sinks (a) with cartridge heaters.*

Wires are soldered onto copper plates, which in turn are glued (using a cement and silver powder mix) to each electrode. These wires form the fuel cell's link to the external circuit and, with them in place, the fuel cell assembly is complete.

iii. Describing the Experimental Setup:

The PEM fuel cell assembly is placed in an insulating box, along with a gas humidifier. H_2, CO_2, and N_2 gases are run through pressure regulators (the first two come from industrial gas tanks – BOC for H_2 and Airgas for CO_2 – and the last is house N_2) and are then fed to Aalborg® 0-50mL mass flow controllers (MFCs). An O_2 0-50 mL MFC was used in the case of the CO_2 stream, but it was calibrated beforehand to ensure that the proper H_2:CO_2 ratios are investigated. The H_2 and CO_2 streams are then fed to a T-junction, and the mixed gas line is sent to the humidifier within the insulating box. The humidifier's water level is monitored and topped up before each run. Once humidified, the H_2/CO_2 mixture is fed into the anode compartment of the PEM fuel cell. The dry N_2 gas is fed into the cell's cathode compartment without prior humidification. The anode and cathode outlets are channeled to a water bath – they are only removed from this bath when an analysis of outlet gas flow rates and outlet gas compositions is carried out. The fuel cell's cartridge heaters are controlled digitally as mentioned in the previous section, and heat tracing of the gas lines is employed within the insulating box: heating tape covers the humidifier, the humidifier to fuel cell line, the anode outlet to water bath line, and the cathode outlet to water bath line. Temperatures are controlled through variacs for

the first of these two heating tapes, and through digital temperature controllers for the last two. Thermocouples are installed in the fuel cell, the humidifier, the insulating box, the anode inlet, the anode outlet, and the cathode outlet (the last three as part of a relative humidity sensing package from SENSIRON: these were removed once the temperature settings of the different elements were finalized and 100% humidification of the fuel cell was confirmed). The fuel cell's external circuit wires are connected to the Arbin data acquisition system (DAQ) – which doubles as our power supply – and this, in turn, is connected to a desktop computer running the Arbin's MSTAT4+ software, which is responsible for the bulk of our data analysis. Figure 6 provides a schematic of our setup.

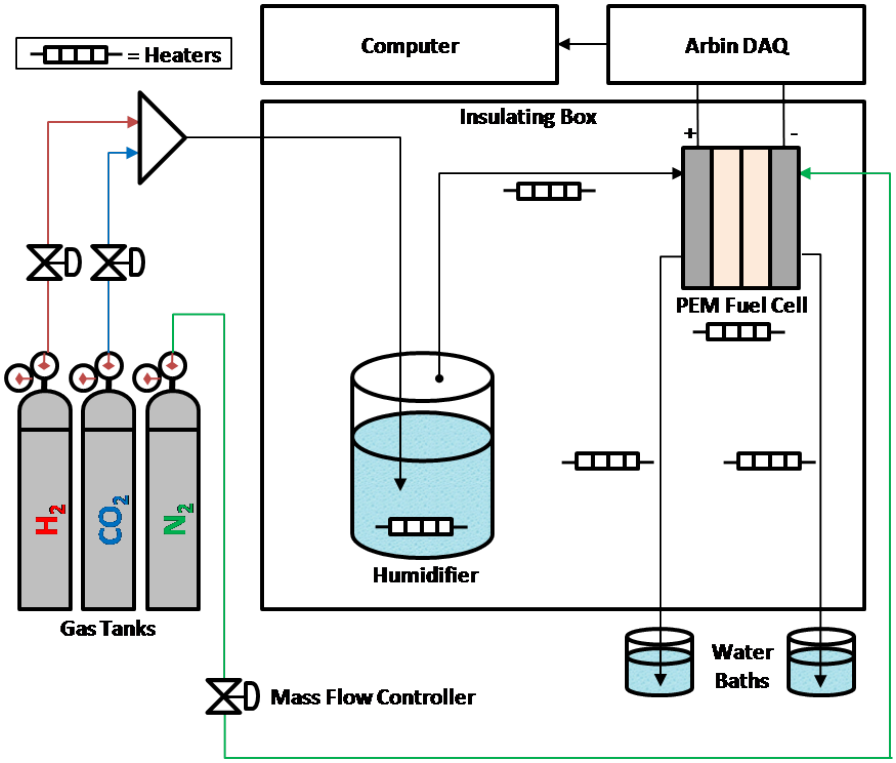

Figure 6: *A schematic of our setup, showing the gas delivery apparatus, as well as the insulating box containing the gas humidifier and the PEM fuel cell assembly. Temperature control techniques are employed at the humidifier, fuel cell, anode inlet, anode outlet, and cathode outlet.*

iv. Data Acquisition Techniques:

As mentioned earlier, the main system for data analysis is the Arbin DAQ's MSTAT4+ software. The Arbin is capable of running schedules that involve current ramps, current holds, voltage ramps, voltage holds, and membrane R_{int} checks using the current-interrupt method. It can provide the necessary information for determining the degree of poisoning the membrane experiences from the CO_2 molecules at different currents, temperatures, and gas stream compositions.

The Arbin cannot, however, tell us how efficient our separation is. It can give no experimental verification of hydrogen pumping, or indeed of hydrogen yield or separation efficiency. Therefore, an HP 0104-0113 soap film flowmeter is used to measure the amount of hydrogen pumped from anode to cathode given the flow rates at the anode and cathode outlets.

To determine how much CO_2 is present at the anode and cathode outlets, two variations of Sensidyne's Precision Gas Detector Tubes (GDTs) are used: the 126UH model is used to measure CO_2 concentration at the anode, since it can detect concentrations of 5v% to 50v% CO_2, and, at the cathode, we use the 126 SG model which has a much finer detection range of 0.02v% to 1.4v% CO_2. GDTs are graduated tubes containing a fixed bed of reactant that, upon contact with CO_2, changes color. The combination of graduated tube and color change helps determine the percentage volume of CO_2 in a 50mL sample of air. In each case, 50mL of the outlet gas is collected (it is either collected in a syringe or by capturing it in an inverted graduated cylinder) and fed into the appropriate tube.

Arbin schedules range from five to ten hours, with each current hold lasting for 30 minutes, after which an R_{int} check is performed and the current hold is continued (or a different current applied). Between current cycles, the potential across the membrane is forced to 0V using Arbin's voltage hold step to counter the effects of concentration polarization, and to negate mass transport limitations that might degrade cell performance by requiring a higher potential difference to be applied in order to maintain a constant current. Five types of runs are performed: (i) runs with hydrogen at 54°C (FC temperature) at 0.5A and 1.0A, (ii) runs with hydrogen at 74°C at both currents, (iii) runs with a 3:1 H_2:CO_2 mixture at 54°C and both currents, (iv) runs with a 3:1 H_2:CO_2 mixture at 74°C and both currents and, lastly, (v) runs at 54°C and a current of 1.0A during which the H_2:CO_2 ratio is varied from 3:1 to 2.5:1, to 2:1, to 1.5:1, to 1:1, and lastly to 0.5:1 to simulate a theoretical 100% hydrogen recovery. This last run will be referred to henceforth as the multiple differential element simulation (MDES) – or stack simulation.

Part IV – Results and Discussion

i. The Effect of Temperature on Hydrogen Pumping:

As a control experiment, the PEM fuel cell was run with pure hydrogen as its only feed at the anode and at a temperature of 54°C. Arbin cycled between an applied current of 0.5A and 1.0A and, every 60s, it recorded the potential difference across the membrane. Using Arbin's data, we can construct a graph of voltage versus time which will tell us how much power the fuel cell requires for hydrogen pumping, as well as whether its performance is degrading over time (a phenomenon that is attributed to

concentration polarization within the MEA). Similarly, we can compare the R_{int} measured by Arbin using its current-interrupt method to the average resistance calculated through averaging the voltage data acquired by Arbin.

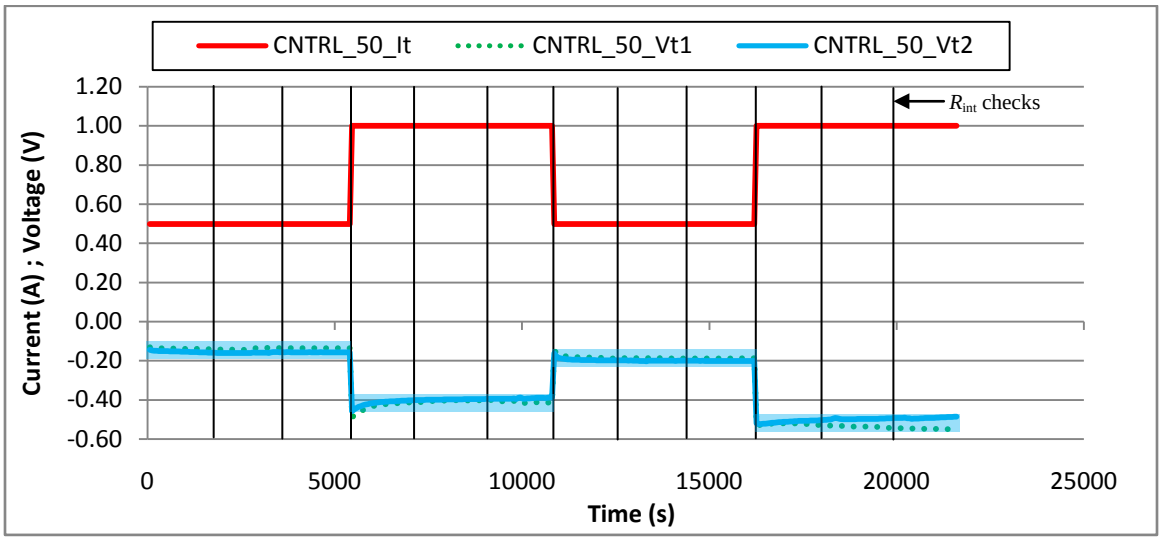

Figure 7: *A current (A) and voltage (V) versus time graph for the 54°C H_2 pumping control experiments. The graph shows constant fuel cell performance. H_2 flow rate = 48mL/min, N_2 flow rate = 12mL/min. The error region is shaded for each run.*

Figure 7 shows both current and voltage as functions of time. The former is represented by the line denoted (It), while the potential recorded by Arbin during two separate runs is represented by the lines denoted (Vt1) and (Vt2). Arbin adopts a convention whereby any 'applied' power is negative, hence the negative voltage figures recorded above. Data will be presented according to this convention, except where noted. Figure 7 shows no substantial degradation in the hydrogen pumping capacity over time. The degradation in performance between the first 0.5A and 1.0A cycle and the second one can be attributed to concentration polarization: as the hydrogen is consumed by the reaction at the anode, a greater change in potential is required to maintain the current (mass transport limitations come into play). The runs were repeated and the voltage between the two cycles zeroed. The results of those runs show consistent potential

measurements over time with no degradation in performance. The H_2 flow rate at the anode was 48mL/min, while the N_2 flow rate was 12mL/min. At 0.5A, the average anode outlet flow rate $\dot{n}(\overline{A_o})$ was 44mL/min ± 0.5mL/min, while the cathode's outlet $\dot{n}(\overline{C_o})$ was at 15.9mL/min ± 0.1mL/min. A mass balance tells us that 3.8 to 4.0mL/min of H_2 was pumped across the membrane, which is consistent with theoretical predications of fuel cell operation at these conditions. At 1.0A, $\dot{n}(\overline{A_o})$ was 40mL/min ± 0.5mL/min, and $\dot{n}(\overline{C_o})$ was 19.9mL/min ± 0.1mL/min, which suggests that between 7.8 and 8mL/min of H_2 was pumped across the membrane, again matching expectations.

The hydrogen yield, η_H, which is defined as the ratio of recovered to fed H_2, H_R/H_F, is thus equal to 0.08 (8%) at 0.5A and 0.17 (17%) at 1.0A. The cell's power requirements are – expectedly – very low at these relatively low currents: at 0.5A, the average power requirement P_{av} was 504W/mol H_2 recovered while, at 1.0A, it increased to 1288W/mol H_2 recovered. There are two calculations regarding power that need to be explained. The first, P_{av}, is merely the product of I and V_{avg}, the latter being the average of the voltage at a particular I as calculated by Arbin for every 30 minute current hold, as outlined in table 1 below. The second calculation is the calculation of the power required to drive the reactions at the two electrodes (the overpotential loss), or P_{OPL}, which can be deduced by looking at the difference between the power required for ion transport $P_{ion} = I^2 R_{int}$ and the thermodynamic power requirement $P_{thermo} = IV_{thermodynamic}$.

Table 1: *V_{avg} and P_{av}, as defined in the discussion above, for both 54°C control runs.*

Run Number	**1**				**2**			
Cycle Number	**Cycle 1**		**Cycle 2**		**Cycle 1**		**Cycle 2**	
I (A)	*0.50*	*1.0*	*0.50*	*1.0*	*0.50*	*1.0*	*0.50*	*1.0*
V_{avg} (V)	*0.14*	*0.42*	*0.19*	*0.53*	*0.16*	*0.40*	*0.20*	*0.50*
P_{av} (W)	*0.07*	*0.42*	*0.10*	*0.53*	*0.08*	*0.40*	*0.10*	*0.50*

Both P_{ion} and P_{thermo} are calculated for each current hold using the equations presented above and, knowing the values of both, we can also calculate the power required to drive the kinetics of the reactions at both anode and cathode, P_{OPL}, as figure 8 below illustrates:

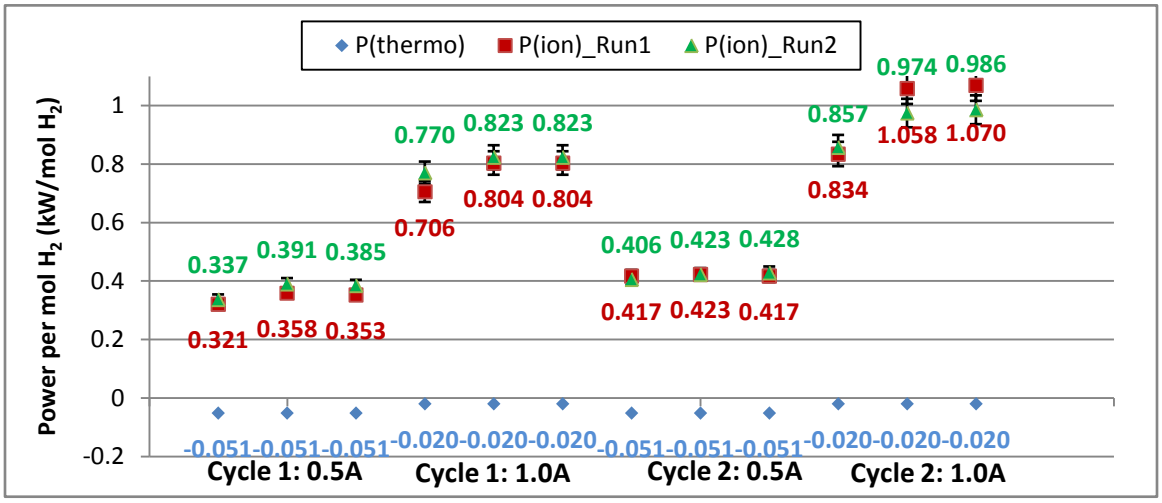

Figure 8: *An illustration of the difference between the thermodynamic power given off by the cell's operation and the power required for ion transport. The power required for the electrode reactions (P_{OPL}) is the difference between these two values. The sign convention differs from Arbin's.*

Figure 8 shows how the thermodynamic power requirement is negative (in other words, the H_2 pump actually provides a small potential that drives the reactions). This is due to the higher H_2 partial pressure at the anode relative to the cathode. Nevertheless, power is *required* (positive) for ion transport across the membrane, as both runs confirm. The difference between these two values, P_{OPL}, is therefore the power required to drive the reactions at the two electrodes of the cell.

The cell efficiency, η_{cell}, is defined as the ratio of H_2 recovered to H_2 produced theoretically (which is solely a function of current intensity). At a current of 0.5A, η_{cell} was equal to 95.9% while, at 1.0A, η_{cell} was equal to 95.3%. This suggests that the volume of H_2 pumped across the membrane is close – but not equal – to that expected.

Since the setup was checked consistently for leakages, the only possible explanation for these discrepancies is an error in measurement.

An analysis of R_{int} vs. R_{avg} (the average resistance as calculated from Arbin's voltage measurements) shows that R_{avg} is always higher than R_{int}. The difference between the two values ranges from 10% to 40%, as figure 9 shows, with the two values diverging noticeably more during current holds at 1.0A compared to those at 0.5A.

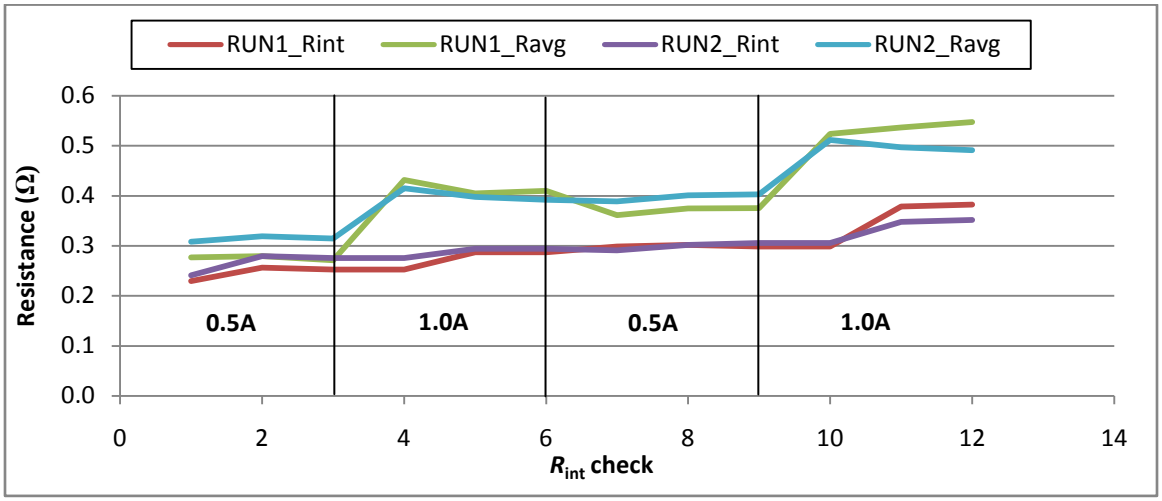

Figure 9: *R_{int} vs. R_{avg} at different current holds throughout the two control runs. R_{avg} increases markedly with increasing current, and the discrepancies between the two values are greatest at the 1.0A cycles.*

One possible explanation for these discrepancies is the fact that R_{avg} figures, which are calculated from V_{avg} data acquired by Arbin, do not eliminate the ohmic losses that are associated with fuel cell operation. These inevitable ohmic losses increase the potential required for the hydrogen pumping operation and, the greater the pumping capacity demanded of the electrochemical cell, the higher the applied potential and the greater the ohmic losses associated with cell operation. The R_{int} figures, on the other hand, are recorded during abrupt current-interrupt steps. When the current is reduced to zero rapidly, as it is in such steps, the cell returns to open circuit conditions for an instant, which immediately eliminates ohmic losses [33].

One thing to note is the apparent lag between the change in R_{avg} and the change in R_{int}. As figure 9 clearly shows, once the voltage is increased from 0.5A to 1.0A after the third R_{int} check, the R_{avg} increases, as expected, to reflect the increased potential applied to the cell in order to maintain the higher current of 1.0A. R_{int}, however, remains more or less constant during the first current hold at 1.0A. The higher internal resistance of the cell is only registered after the second current hold (R_{int} check 5). One possible reason for this behavior is the slow rearrangement of charge distribution in the membrane itself. This rearrangement continues throughout the first two current holds until the cell's performance stabilizes one hour into the current hold. This pattern is seen throughout the investigation and, because it lies well outside of our problem description and the nature of our experimental setup, it cannot be studied further. Nevertheless, it is noted here in the hope that future studies into the nature of this phenomenon will be carried out.

From figure 9, we can also see that the power requirements for the cell, which are calculated using IV_{avg} or I^2R_{avg}, are greater in magnitude than I^2R_{int}. The discrepancy between the two values is greater at 1.0A than it is at 0.5A.

The same experiment – with the same Arbin test schedule – is repeated at a fuel cell temperature of 74°C. Figure 10 shows the results of two such runs and, as in the previous case, there is no evidence of substantial degradation in fuel cell performance over time. The runs show remarkable reproducibility:

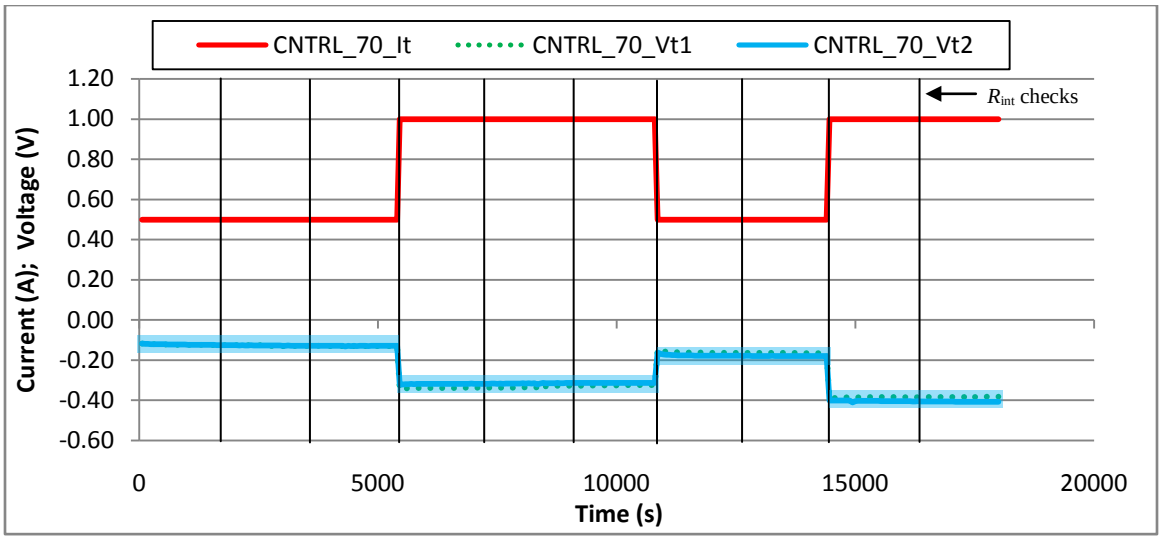

Figure 10: *A current (A) and voltage (V) versus time graph for the 74°C H_2 pumping control experiments. The graph shows constant fuel cell performance. H_2 flow rate = 48mL/min, N_2 flow rate = 12mL/min. The error region is shaded for each run.*

Little variations in hydrogen pumping were witnessed between the two temperatures. Any variations in temperatures are accounted for entirely by differences in internal membrane condition at the start of each run. This is precisely what is expected, since hydrogen pumping capacity is dependent solely on applied current. At 0.5A, $\dot{n}(\overline{A_o})$ was 44mL/min ± 0.5mL/min, while $\dot{n}(\overline{C_o})$ was 15.9mL/min ± 0.1mL/min: 3.9mL/min of H_2 was therefore pumped across the membrane. At 1.0A, the flow rate at the anode was 40mL/min ± 0.5mL/min and, at the cathode, between 20 mL/min ± 0.1mL/min. 8mL/min of H_2 was pumped across the membrane. η_H and η_{cell} are consistent with those calculated for the previous runs where the temperature was 54°C.

Table 2: *V_{avg} and P_{av} for both 74°C control runs.*

Run Number	**1**				**2**			
Cycle Number	**Cycle 1**		**Cycle 2**		**Cycle 1**		**Cycle 2**	
I (A)	*0.50*	*1.0*	*0.50*	*1.0*	*0.50*	*1.0*	*0.50*	*1.0*
V_{avg} (V)	*0.13*	*0.33*	*0.16*	*0.39*	*0.13*	*0.32*	*0.18*	*0.41*
P_{av} (W)	*0.06*	*0.33*	*0.08*	*0.38*	*0.06*	*0.32*	*0.09*	*0.40*

Figure 11, like figure 8, shows how, at 1.0A, the power required for reactions at the electrode surfaces increases fourfold compared to the power requirements at 0.5A:

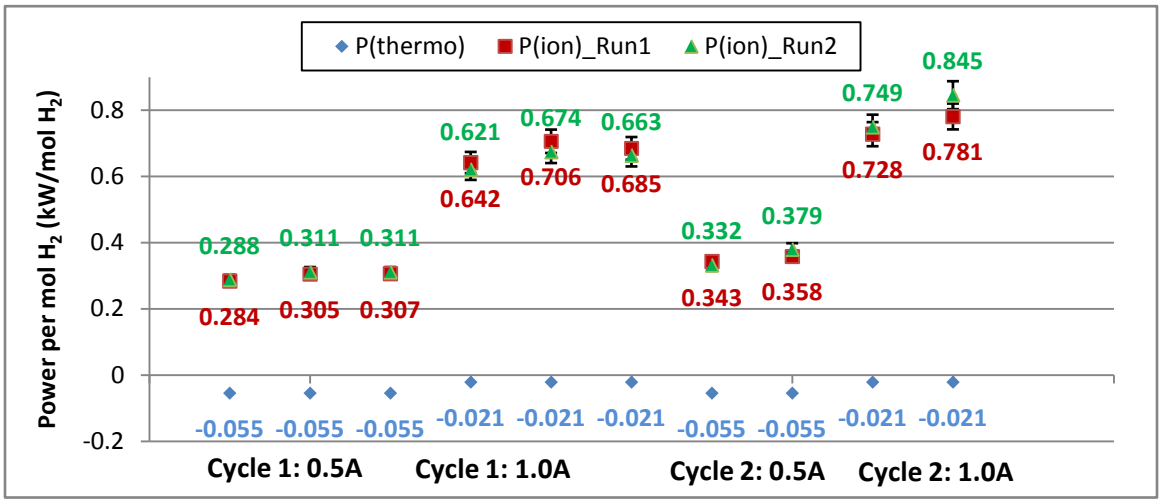

Figure 11: *An illustration of the difference between the thermodynamic power given off by the cell's operation and the power required for ion transport. The power required for the electrode reactions (P_{OPL}) is the difference between the two values. The sign convention differs from Arbin's.*

Once the control runs established the electrochemical cell's performance characteristics with pure H_2 as the anode feed, a mixture of 3:1 H_2:CO_2 was introduced at the anode. This corresponded to H_2 and CO_2 flow rates of 48mL/min and 16mL/min, respectively. The Arbin test schedules employed for these runs were similar to those used above, with the potentials at currents of 0.5A and 1.0A recorded for analysis.

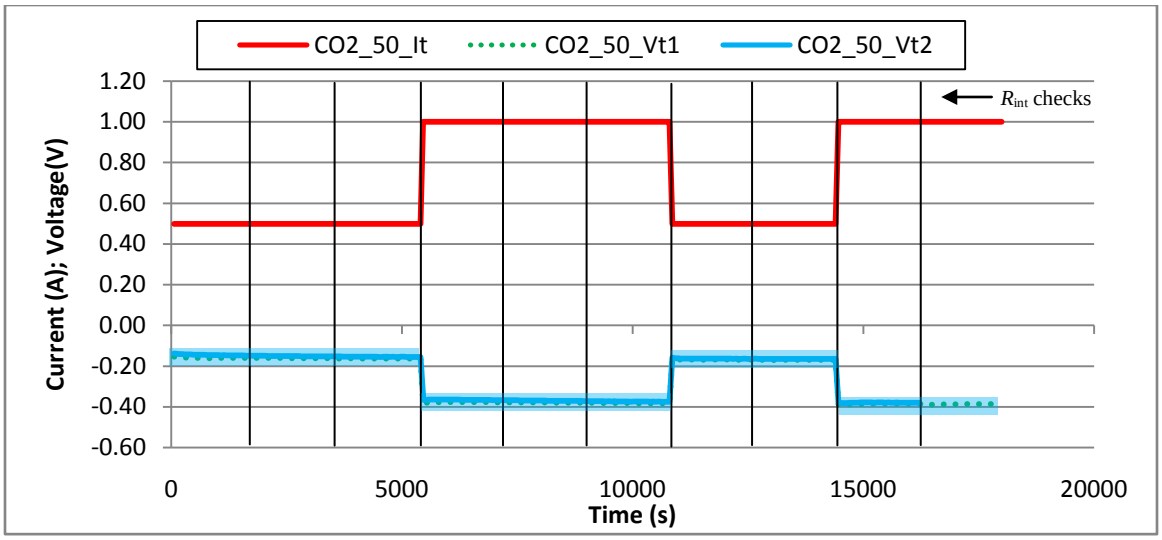

Figure 12: *A current (A) and voltage (V) versus time graph for the 54°C 3:1 H_2:CO_2 pumping experiments. The graph shows little degradation in FC performance. H_2 flow rate = 48mL/min, CO_2 flow rate = 16mL/min, N_2 flow rate = 12mL/min. The error region is shaded for each run.*

The results of these runs show some degradation of fuel cell performance over time. Unlike the control runs discussed previously, the magnitude of the potential at the end of each current hold is greater than the potential at its start. Both runs show that the potential required to pump hydrogen across the membrane increases over time. Table 3 illustrates the extent of this degradation in performance.

Table 3: *Unlike in the control runs, it was clear that the driving force required to pump hydrogen across the membrane when the mixture included CO_2 increased over time. The voltage increase is the percentage increase in the magnitude of the voltage at the end of each current hold compared to its start. The error governing V_{avg} (which translates to 1%) is propagated to the P_{av} calculation, but is not incorporated here.*

Run Number	**1**				**2**			
Cycle Number	**Cycle 1**		**Cycle 2**		**Cycle 1**		**Cycle 2**	
I (A)	*0.5*	*1.0*	*0.5*	*1.0*	*0.5*	*1.0*	*0.5*	*1.0*
V increase (%)	*6.5*	*1.6*	*1.2*	*-0.3*	*11*	*2.7*	*1.9*	*0.5*
V_{avg} (V)	*0.16*	*0.38*	*0.17*	*0.39*	*0.14*	*0.37*	*0.16*	*0.38*
P_{av} (W)	*0.08*	*0.38*	*0.09*	*0.39*	*0.07*	*0.37*	*0.08*	*0.38*

Between cycles 1 and 2 of each run, the voltage was forced to zero, which would replicate open circuit conditions. The voltages recorded at the start of the 0.5A current hold of cycle 2 were 0.164 V and 0.159 V for runs 1 and 2, respectively. This contrasted with the voltages recorded at the start of the 0.5 current hold of cycles 1, which were

0.153 V and 0.138 V for runs 1 and 2, respectively. In other words, the potential required to pump hydrogen increased by 7.2% during run 1 and by 15% during run 2. Since similar increases of voltage (of between 5 and 15%) were recorded for the control run, we can conclude that no permanent poisoning of the PEM was seen at the conditions examined, and that the increases in voltage were due to the fact that the membrane was not allowed to relax thoroughly between cycles as it did before the run was initiated every morning.

At 0.5A, $\dot{n}(\overline{A_o})$ was 60mL/min ± 0.5mL/min, while $\dot{n}(\overline{C_o})$ flowed at 16mL/min ± 0.1mL/min; again, 4.0mL/min of H_2 was pumped across the membrane, which is consistent with theoretical predictions of fuel cell operation at these conditions. At 1.0A, $\dot{n}(\overline{A_o})$ was 56mL/min ± 0.5mL/min, and $\dot{n}(\overline{C_o})$ was 20mL/min ± 0.1mL/min, which suggests that 8mL/min of H_2 was pumped across the membrane. η_H is equal to 0.08 (8%) at 0.5A and 0.17 (17%) at 1.0A. The cell's power requirements were again very low at these relatively low currents, but they did increase over time, reflecting the higher potential required to transport the H_2 from anode to cathode. At 0.5A, P_{av} increased between 6% and 12% from the start of the first current hold to the end of the second current hold of each run, while, at 1.0A, the power requirement increased between 2% and 4%, despite the higher ohmic losses associated with these runs. The increases in power requirements follow the pattern of those witnessed in the control runs, and can be explained by the increase in the PEM's internal resistance as the run proceeded. Again, this does not necessarily indicate that carbon dioxide poisoning hampers cell performance at these conditions like carbon monoxide poisoning has been proven to. η_{cell} was equal to 95.9% at both 0.5A and 1.0A.

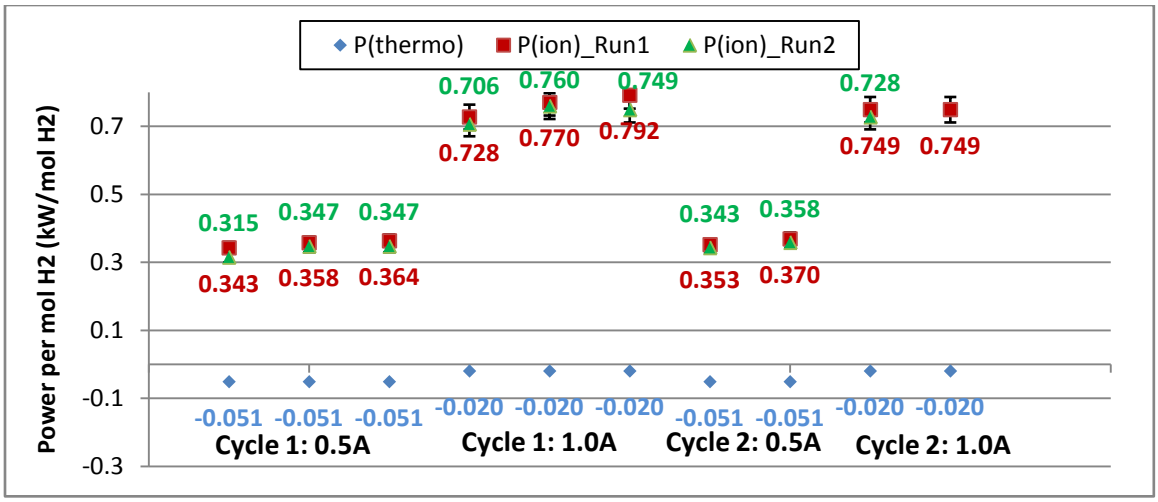

Figure 13: *Power required for the electrode reactions (P_{OPL}) is given for each current hold of each cycle. Also given are P_{thermo} and P_{ion}, from which P_{OPL} is calculated. The sign convention differs from Arbin's.*

An analysis of a 50mL sample of the anode outlet stream via a GDT showed that, at a current of 0.5A, the concentration of CO_2 was 26v%. A mass balance around the fuel cell verifies this reading, as figure 14 illustrates:

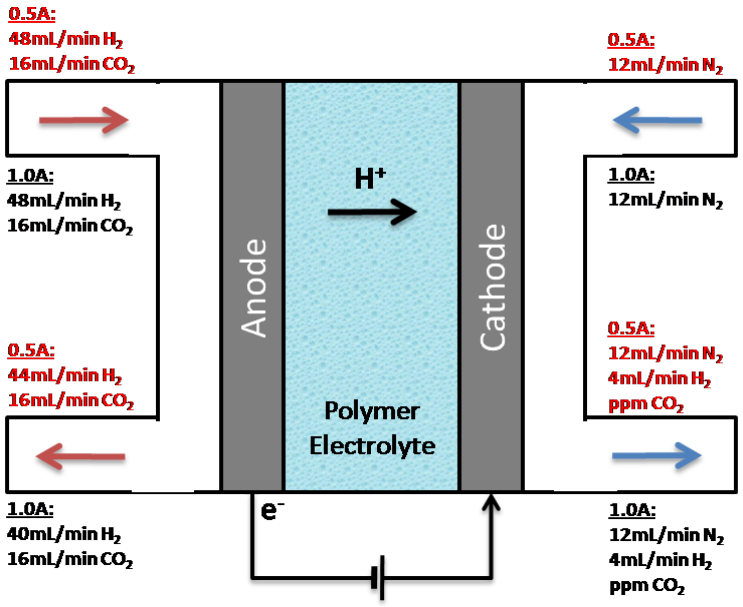

Figure 14: *A representation of electrochemical cell separation as determined at both 0.5A and 1.0A.*

The GDTs also showed that, at the cathode outlet, the concentration of CO_2 was less than the GDT's lower bound of 0.02v%. Since the outlet stream's volume is 16mL,

the lower bound of 0.02v% represents a CO_2 flow rate of $3.2x10^{-4}$ mL/min or 200ppm. We can also define a separation efficiency, η_{sep}, as the percentage of CO_2 removed from the stream entering the anode:

$$\eta_{sep} = \frac{\left(n_{CO_2}^{anode} - n_{CO_2}^{cathode}\right)}{n_{CO_2}^{anode}} \times 100$$

where $n_{CO_2}^{anode}$ is the amount of CO_2 entering the cell at the anode and $n_{CO_2}^{cathode}$ is the amount of CO_2 leaving the cell at the cathode. The lower bound of GDT detection, 0.02v% of CO_2 thus represents a separation efficiency η_{sep} of 99.98%. Since the percentage CO_2 at the cathode was below this threshold, we conclude that operating the cell at these mild conditions will generate an H_2 stream at the cathode that is of purity greater than 99.98%. At a current of 1.0A, the GDTs registered a CO_2 concentration of 28v% at the anode outlet and a concentration of 0.02v% at the cathode outlet. The cathode outlet stream is thus of 99.98% purity even at the higher current setting.

The same trends were observed during the runs performed at 74°C. However, the degradation in performance at 1.0A was noticeable during both runs.

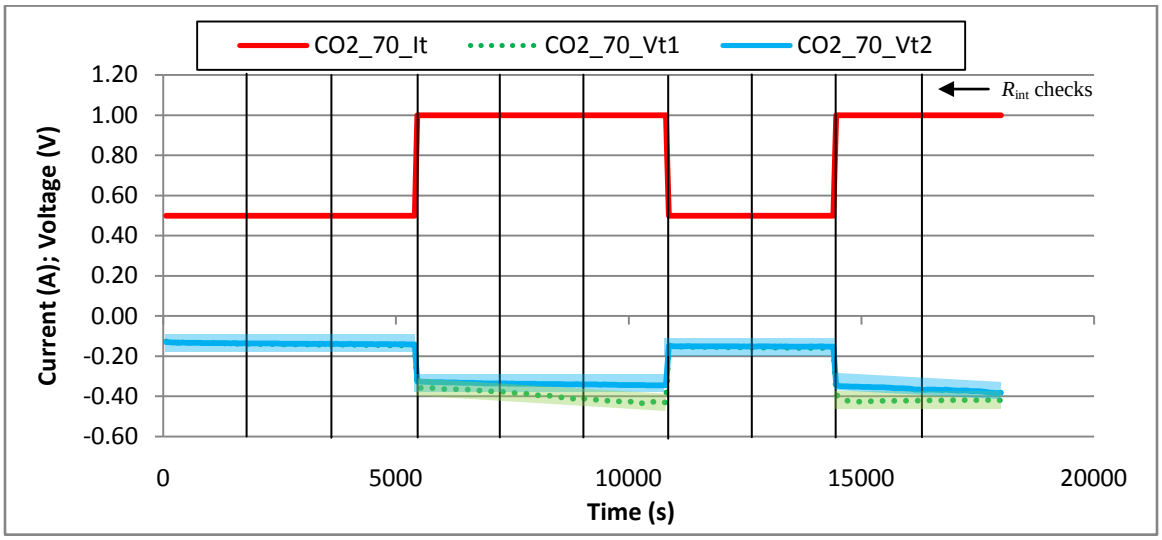

Figure 15: *A current (A) and voltage (V) versus time graph for the 74°C 3:1 H_2:CO_2 pumping experiments. The graph shows some degradation in FC performance. H_2 flow rate = 48mL/min, CO_2 flow rate = 16mL/min, N_2 flow rate = 12mL/min. The error region is shaded for each run.*

Table 4: *The potential required to pump hydrogen across the PEM increases at the end of each current hold, indicating degradation in fuel cell performance. The voltage increase is the percentage increase in the magnitude of the voltage at the end of each current hold compared to its start. The error governing V_{avg} (which translates to 1%) is propagated to the P_{av} calculation, but is not incorporated in this table.*

Run Number	**1**				**2**			
Cycle Number	**Cycle 1**		**Cycle 2**		**Cycle 1**		**Cycle 2**	
I (A)	*0.5*	*1.0*	*0.5*	*1.0*	*0.5*	*1.0*	*0.5*	*1.0*
V increase (%)	*15*	*22*	*6.7*	*7.2*	*8.5*	*5.8*	*4.1*	*11*
V_{avg} (V)	*0.14*	*0.39*	*0.16*	*0.42*	*0.14*	*0.34*	*0.15*	*0.37*
P_{av} (W)	*0.07*	*0.39*	*0.08*	*0.42*	*0.07*	*0.34*	*0.08*	*0.37*

At 0.5A, $\dot{n}(\overline{A_o})$ was 60mL/min ± 0.5mL/min, while $\dot{n}(\overline{C_o})$ flowed at 16mL/min ± 0.1mL/min, indicating that 4.0mL/min of H_2 was pumped across the membrane. At 1.0A, $\dot{n}(\overline{A_o})$ was 56mL/min ± 0.5mL/min, and $\dot{n}(\overline{C_o})$ was 20mL/min ± 0.1mL/min; therefore, 8mL/min of H_2 was pumped across the membrane. η_H is equal to 0.08 (8%) at 0.5A and 0.17 (17%) at 1.0A, much like in earlier runs at different conditions. The cell's power requirements were low at these relatively low currents, but they did increase over time, reflecting the higher potential required to transport the H_2 from anode to cathode.

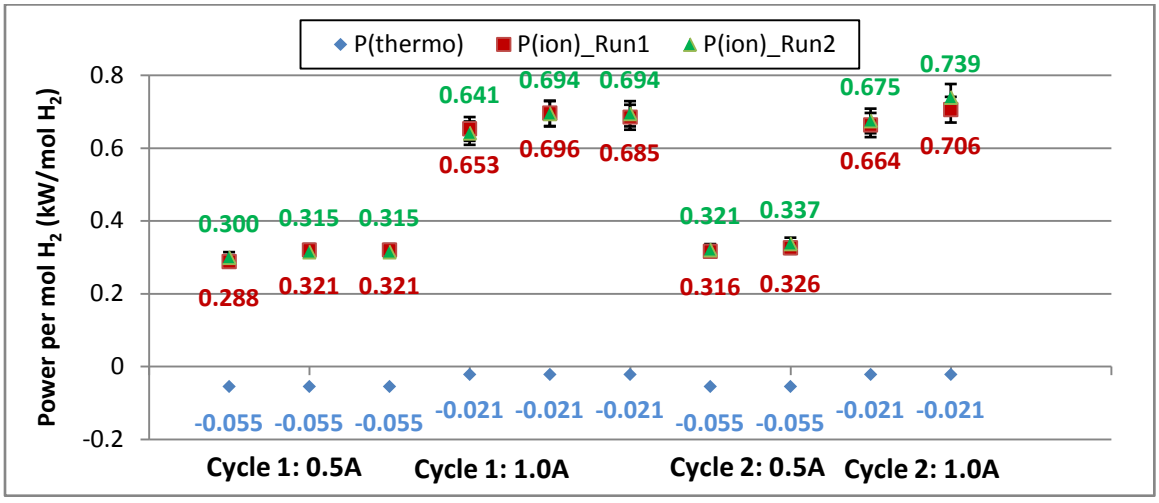

Figure 16: *Power required for the electrode reactions (P_{OPL}) is given for each current hold of each cycle. Also given are P_{thermo} and P_{ion}, from which P_{OPL} is calculated. The sign convention differs from Arbin's.*

At 0.5A, P increased between 13% and 18% between the start of the first current hold and end of the second current hold of each run, while, at 1.0A, the power requirement increased between 12% and 15%. The increases in power requirements at the high temperature runs are therefore only slightly higher than those witnessed during the runs at 54°C. η_{cell} was equal to 97.3% at 0.5A and 94.4% at 1.0A.

Like the H_2 yield, and η_{cell}, analysis of the gases at the anode and cathode outlet streams via the GDTs showed that, at a current of 0.5A, the concentration of CO_2 at the anode and cathode was 26v% and <0.02v%, respectively. At 1.0A, the concentrations were 28v% and 0.02v% at the anode and cathode outlets, respectively.

We can therefore conclude from these runs that, at 54°C, performance degradation upon the introduction of 25v% CO_2 is minimal while, at 74°C, the degradation is more obvious and continues throughout the current hold, especially at higher currents, as figure 17 confirms. This conclusion seems to support the proposition that the RWGS mechanism governs cell performance. As temperature increases, the RWGS reaction (25) is favored and its equilibrium shifts to the right, favoring the formation of CO, which poisons the membrane and degrades fuel cell performance. This is made more likely by the existence of an H_2-rich environment at the anode.

Furthermore, no differences in H_2 pumping, η_{cell}, or H_2 purity at the cathode outlet were seen throughout the investigation. This is precisely what was expected before the investigation was initiated.

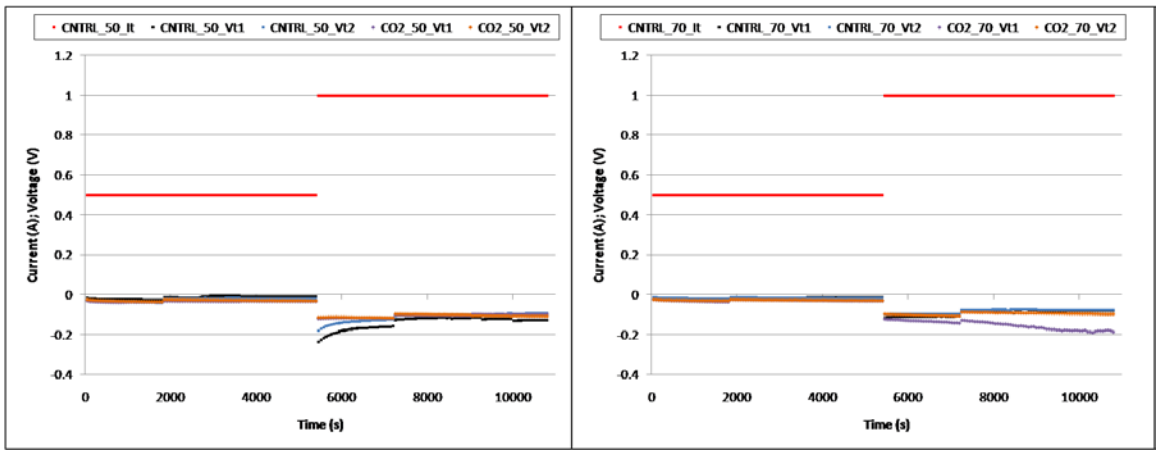

Figure 17: *A plot of the corrected voltage (V_{avg}-IR_{int}) for cycle 1 of fuel cell operation at 54°C (left) and 74°C (right). The degradation witnessed at 54°C is negligible when compared to the control runs while, at 74°C, the degradation is more obvious during both runs.*

ii. A Simulation of a Stack of PEM Differential Elements:

An analysis of the effect of stream composition on fuel cell performance is also performed. An Arbin schedule with multiple 30 minute current holds at 1.0A is set up. The run is started with a 3:1 (48mL/min:16mL/min) H_2:CO_2 mixture at the anode inlet. After 120 minutes of operation, the H_2 flow rate is decreased to 40mL/min, in effect changing the composition of the mixture at the anode's inlet to 2.5:1 H_2:CO_2. After two hours at this composition, the H_2 flow rate is once again decreased to 32mL/min, then to 24mL/min. On one occasion, the flow rate was further reduced to 16mL/min and 8mL/min H_2. The behavior of the potential to these changes in composition is noted. The purpose of this experiment is to determine how feasible maximum hydrogen recovery is at 1.0A. Since we determined that fuel cell operation at 54°C and 1.0A requires little power and does not lend itself to substantial poisoning of the membrane, it would be wise

to maximize H_2 yield by linking 6 such pumps in series. Although we used one cell to simulate this process, figure 18 shows how such a setup would work in practice:

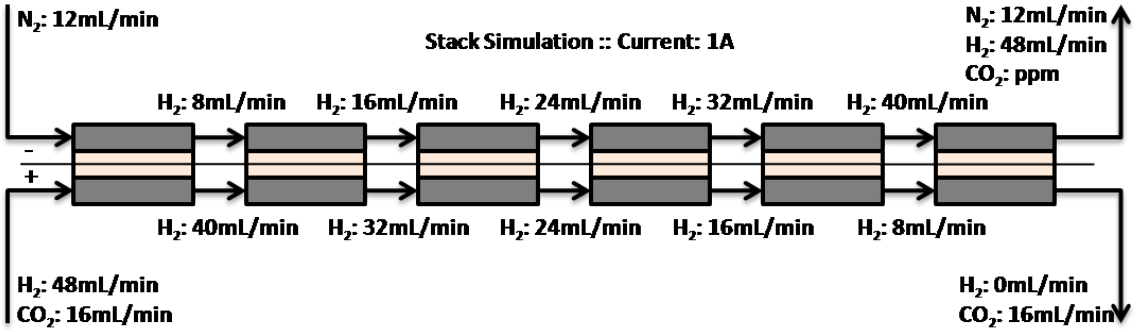

Figure 18: *A stack of electrochemical pumps that should recover 100% of H_2 injected at the anode.*

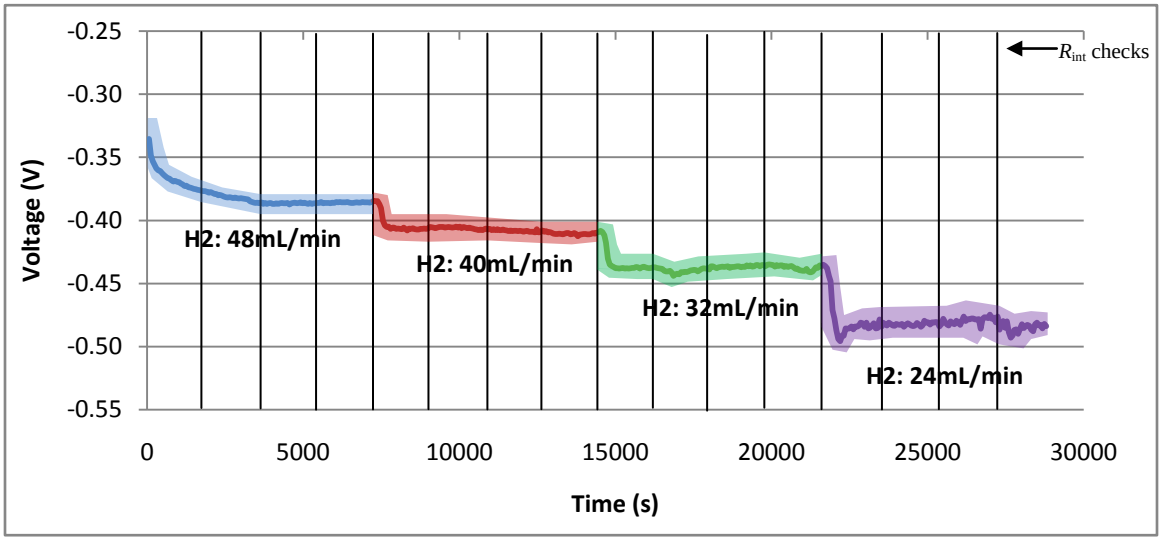

Figure 19: *A simulation of a stack of PEM cells pumping hydrogen at 1.0A, CO_2 flow rate = 16mL/min, and N_2 flow rate = 12mL/min. Potentials increase as H_2 flow rate decrease, and performance becomes more erratic, most likely due to H_2 dilution. FC temperature was 54°C. Error region is shaded.*

At an H_2 flow rate of 48mL/min, $\dot{n}(\overline{A_o})$ was 56mL/min ± 0.5mL/min, and $\dot{n}(\overline{C_o})$ was 19.8mL/min ± 0.1mL/min. When the H_2 flow rate was reduced to 40mL/min, $\dot{n}(\overline{A_o})$ became 48mL/min ± 0.5mL/min, while $\dot{n}(\overline{C_o})$ remained 19.8mL/min ± 0.1mL/min. At 32mL/min H_2, $\dot{n}(\overline{A_o})$ was reduced to 40mL/min ± 0.5mL/min, while $\dot{n}(\overline{C_o})$ was

20.0mL/min ± 0.1mL/min and, at 24mL/min, $\dot{n}(\overline{A_o})$ was 32mL/min ± 0.5mL/min and $\dot{n}(\overline{C_o})$ was 20.0mL/min ± 0.1mL/min.

If we were dealing with a stack of 4 cells, η_H would have thus been equal to 67%. The cell's power requirements increased as the CO_2 concentration in the feed increased, as expected. Also, the behavior of the potential became more erratic as CO_2 concentration increased, which, given the fact that the cell's performance was restored to its original condition after the run without either current pulsing or an air bleed, most likely suggests that the dilution of H_2 is the factor most responsible for the degradation in the cell's performance, as opposed to CO poisoning. Figure 20 shows how the power requirements of the cell change as H_2 concentration in the feed decreases:

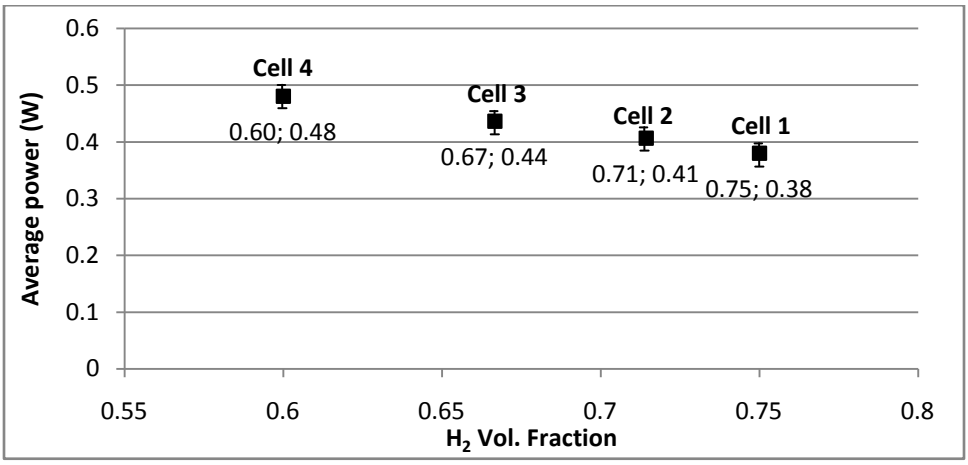

Figure 20: *As the H2 volume fraction in the feed decreases, the power required to operate the cell increases. At the end of this simulation of a 4-cell stack, the hydrogen yield was improved substantially from 17% to 67%.*

The power required to operate this 4-cell stack would therefore be 1.7W, which is 3.5 times the power required to operate one cell. However, the η_H also increased by 300% from a mere 17% to 67%. η_{cell} ranged from 94% to 96% for the four cells. An analysis of the gases at both outlets shows that the CO_2 concentration at the anode increases from 28v% for the first cell (H_2 = 48mL/min) to 33v% for the second cell (H_2 =

40mL/min) to 40v% for the third cell (H_2 = 32mL/min) to 50v% for the fourth cell (H_2 = 24mL/min). At the cathode outlet, the CO_2 concentration increased from 0.02v% for the first cell to 0.03v% for the second cell to 0.04v% for the third cell to 0.06v% for the fourth cell. This indicates that, as CO_2 concentration increases at the anode, diffusion drives more CO_2 molecules to the cathode. If this were a 4-cell stack, the CO_2 volume at the cathode would be 2.40×10^{-2} mL/min, which translates to a CO_2 concentration of 1500ppm. The η_{sep} of such a stack would be 99.85%, which still rivals current industrial methods of hydrogen separation in terms of both purity and separation efficiency.

The last run involved two more feed compositions, a mixture of 1:1 H_2:CO_2 (16mL/min) and a mixture of 0.5:1 H2:CO2 (8mL/min of the former, and 16mL/min of the latter). If we consider the performance seen during the earlier run stable, then these last two feed compositions resulted in vastly more erratic responses in terms of potential, as figure 21 demonstrates.

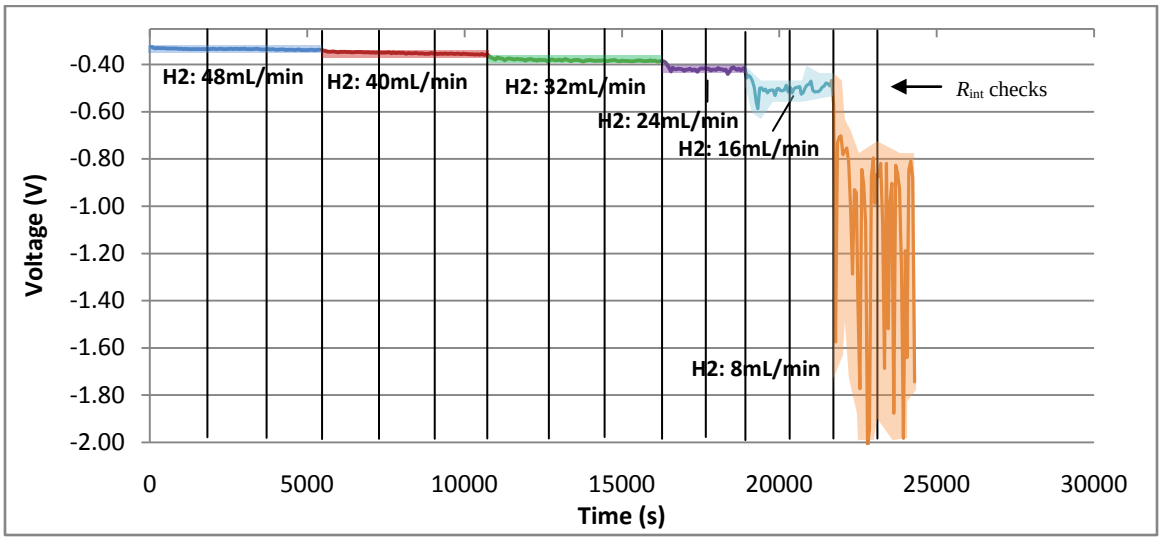

Figure 21: *Despite increasing yield substantially, a 6-cell hydrogen pump operates in an erratic manner compared to the 4-cell pump. The dilution effects become severe when the H_2 flow rate is 8mL/min, as the potential needs to increase dramatically in order to transport most H_2 molecules across the membrane.*

Even at the last two compositions, the cell did manage to pump 8mL/min of H_2 across the membrane. η_{cell} ranged from 93% to 96%, and η_H increased from 67% for the 4-cell stack to greater than 99%. It may be that the erratic behavior at the last setting is due to water being forced into the anode from the humidifier thanks to the vacuum created by the hydrogen pumping procedure, but the experimental apparatus did not lend itself to testing this proposition. The power requirements of cells 1 through 6 relative to H_2 volume fraction are illustrated in figure 22.

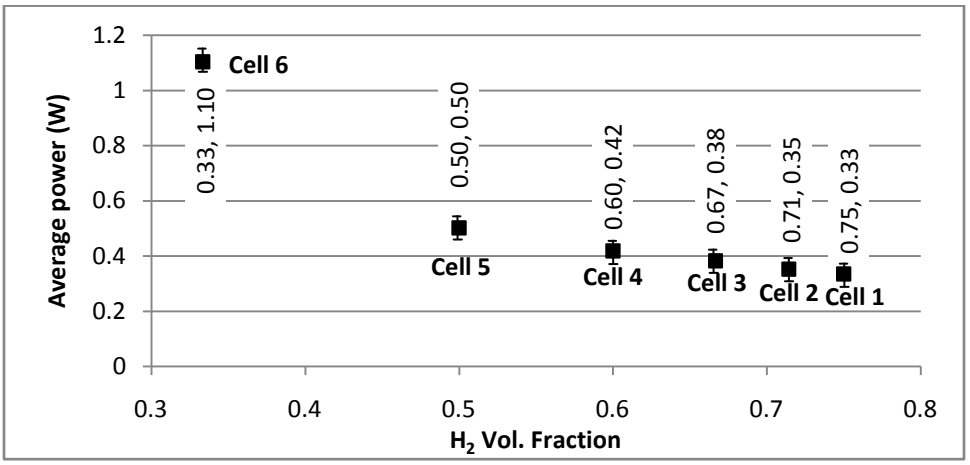

Figure 22: *The power required to operate a 6-cell hydrogen pumping stack increases as the H_2 concentration decreases along the stack. At the exit of a 6-cell stack, the hydrogen yield is virtually 100%.*

The power required for this stack's operation is 3.1W. It represents a greater than 800% increase in power requirement compared to a hydrogen pump composed of just cell 1. η_H does increase by 500% to virtually 100%. As for η_{sep}, the CO_2 concentration at the cathode outlet increased from 0.02v% at cell 1 to 0.08v% at cell 6; diffusion does increase as CO_2 concentration at the anode increases. The overall CO_2 volume at the cathode outlet would be 4.5×10^{-2} mL/min, which translates to 2800ppm.The η_{sep} of such a stack would decrease compared to the 4-cell stack from 99.85% to 99.72%.

Figure 23 demonstrates how insistence on high hydrogen yield has an effect on the purity of the separation. As the feed progresses through a 6-cell stack, η_H increases from 17% (cell 1) to 100% (cell 6), while η_{sep} falls from 99.98% (cell 1) to 99.72% (cell 6), a decline in separation efficiency of less than 0.3%.

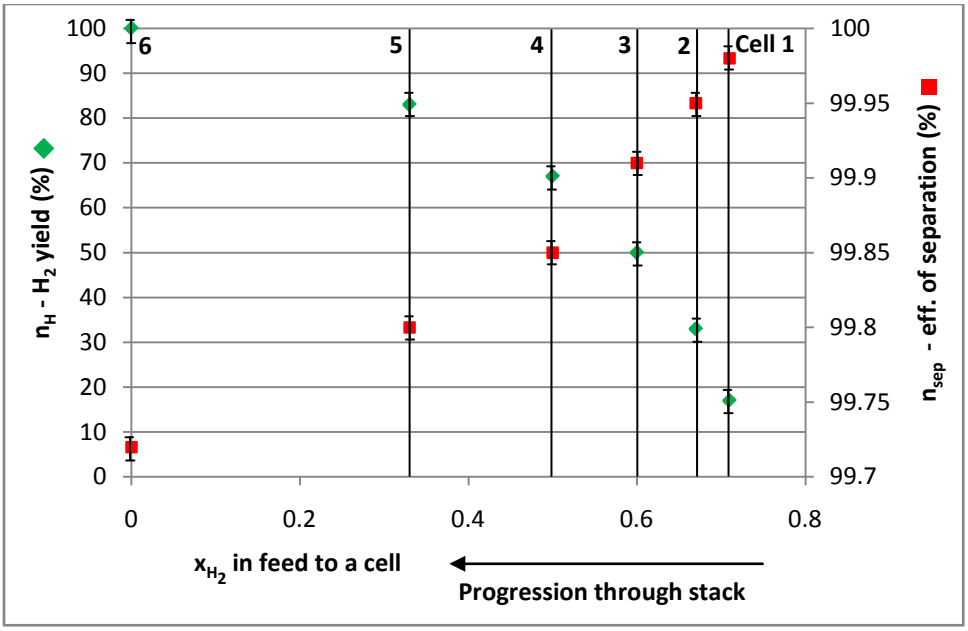

Figure 23: *In a 6-cell stack, hydrogen yield increase as we progress through the stack. Separation efficiency decreases marginally in the process.*

iii. An Investigation into H_2 Pumping's Economic Feasibility:

Now that the empirical results behind our proposal have been established, it becomes necessary to conduct a preliminary economic analysis into the feasibility of our proposed method of separation as opposed to the most common industrial alternative: PSA. Although most H_2 production and separation companies – the most notable being UOP [36] – have probably conducted studies that determine the energy cost incurred per mole of H_2 purified, none of this information is in the public domain as these companies

consider it proprietary [35]. Hence, the only way to proceed with this comparison would be to find the cost required to run a currently-operational PSA complex.

Having worked at such a plant, I was able to contact the chief engineer at the Bahrain Petroleum Company's (BAPCO) Low Sulfur Diesel Production Plant (LSDPP) which generates H_2 through steam reforming and purifies it using PSA as part of a heavy vacuum gas oil (HVGO) hydrocracking complex. The plant cracks 40,000 barrels of HVGO per day. Assuming that the waxes being cracked are heavy alkanes – and that one mole of alkane requires one mole of H_2 to decompose into two lighter alkanes (an assumption that is by no means definitive) – we can deduce that the PSA complex purifies 18,000 moles of H_2 per day. According to the engineer's rough estimates, the operating cost of the complex is $500,000 per annum, or $1,471 per day (assuming it operates for 340 days a year). These figures translate to $0.082 (8₵) per mol H_2 purified.

A 1-cell H_2 pump, on the other hand, consumes 0.33W and has a yield of 8%. Using our setup (and flow rates) as the blueprint for this operation, the cell would purify 1 mole of H_2 every 45 hrs, consuming 1.188 kWh in the process. Assuming the cell is being used in residential applications, we use the U.S. average cost of electricity in our calculations (11₵/kWh). Therefore, it costs $0.13 per mol H_2 purified, which is greater than the cost required for PSA. We must recall that the cost of energy used in the PSA calculation is an order of magnitude lower than that used in this calculation.

This is only the most preliminary of calculations, as it incorporates many assumptions: commercial electricity in Bahrain is cheaper than it is in the U.S., and BAPCO generates its own electricity in its own power stations. The discrepancy in energy costs still holds despite the fact that the cost of commercial electricity in the U.S.

is far less than the 11₵/kWh used in the e lectrochemical pump calculations. The use of this last figure is, we believe, justified; this cell would ultimately be used in localized applications after all.

It is obvious from our previous analysis that, as we insist on higher yields, the power required to operate the stack increases. Figure 24 confirms this trend in terms of both purification energy requirements and their costs:

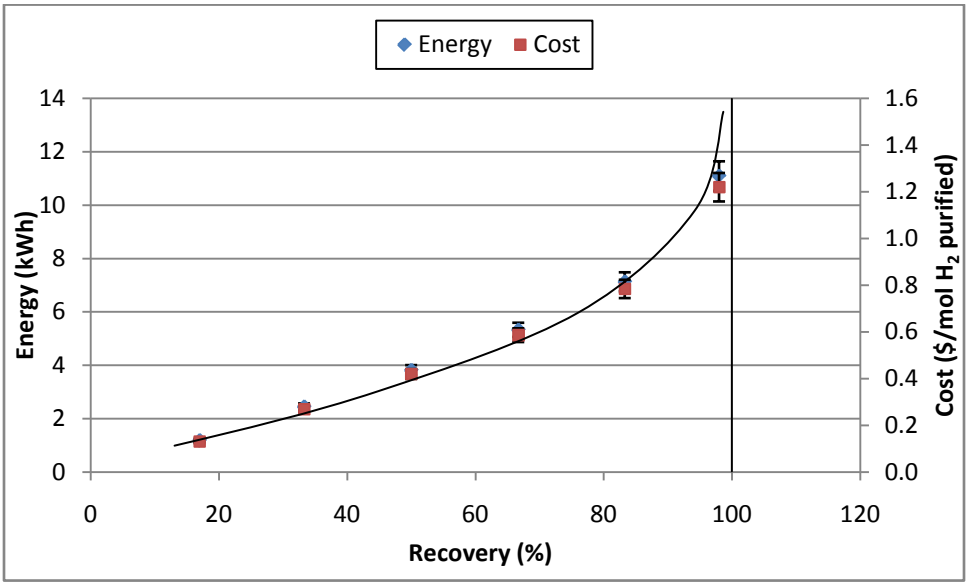

Figure 24: *The higher the recovery rates sought during the pumping operation, the more energy is required to operate the electrochemical pump, and the more costly the process becomes.*

From our discussion of the power requirements for the 4-cell and 6-cell stacks, it appears that there is a tipping point beyond which the cost of the energy required to recover each unit of H_2 is higher than the energy value of the unit of H_2 itself. As figure 25 shows, when the FC stack is expanded from five to six cells, the increase in power requirements outstrips the corresponding increase in H_2 recovery (from 83% to 100%). At every other point along the stack, the difference between the change in power and the corresponding change in yield is 10% or less, while that at the final point (from cell 5 to cell 6) is a considerably larger 36%. The tipping point mentioned earlier occurs at the

point before last, where the trend of decreasing changes in yield accompanied with decreasing changes in power requirement is reversed.

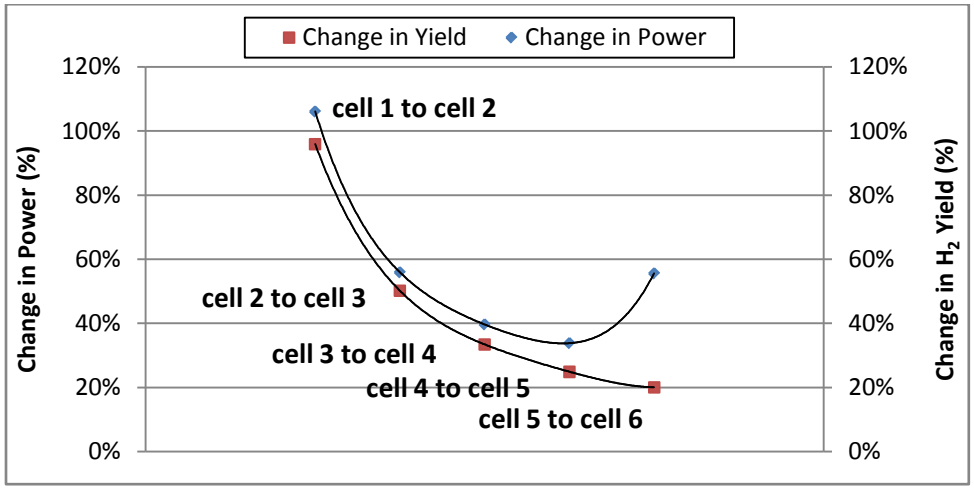

Figure 25: *An analysis of the change in power vs. the change in yield as one progresses through a 6-cell stack electrochemical pumping stack.*

The existence of a tipping point can be established theoretically by proving that, as the rate of recovery approaches 100%, the energy required for the recovery approaches infinity. The graph of energy vs. recovery is thus a reciprocal graph with an asymptote at 100% H_2 recovery. The starting point for this proof should be the mass balance at the anode with the confluence of the anode feed composition, the thermodynamic voltage, and Faraday's law of electrolysis:

$$x_H^{IN} F_A - \frac{P_C}{P_A} \exp\left(\frac{-2\mathfrak{F}V}{RT}\right) F_A = 2\mathfrak{F}I \qquad (27)$$

where x_H^{IN} is the composition of H_2 in the feed, F_A is the feed flow rate, $\mathfrak{F}$ is the Faraday constant, and P_C and P_A are the H_2 partial pressures at the cathode and anode, respectively. If we simply rearrange (27) to solve for the current I, we get:

$$\left(x_H^{IN} - \frac{P_C}{P_A} \exp\left(\frac{-2\mathfrak{F}V}{RT}\right)\right) \frac{F_A}{2\mathfrak{F}} = I \qquad (28)$$

and, knowing that the fraction of H_2 recovered is – by definition – the amount of H_2 pumped across the membrane divided by the amount of H_2 in the feed, we recognize that the fraction of H_2 recovered is simply the expression shown below:

$$\frac{2\mathfrak{F}I}{F_A x_H^{IN}} \tag{29}$$

We can then rearrange (27) to yield an expression for H_2 recovery:

$$\frac{2\mathfrak{F}I}{F_A x_H^{IN}} = \left(1 - \frac{P_C}{x_H^{IN} P_A} \exp\left(\frac{-2\mathfrak{F}V}{RT}\right)\right) \tag{30}$$

We also know that power (P) is merely V multiplied by I:

$$P = IV \tag{31}$$

We can divide (29) by (31) to get an expression for energy efficiency, which we shall define as recovery over power. Therefore,

$$Energy\ Efficiency \propto \frac{1}{V} \tag{32}$$

Equation (27) has several limiting conditions. At $I = 0$:

$$x_H^{IN} - \frac{P_C}{P_A} \exp\left(\frac{-2\mathfrak{F}V}{RT}\right) = 0 \tag{33}$$

$$V = -\frac{-RT}{2\mathfrak{F}} \ln\left(\frac{x_H^{IN} P_A}{P_C}\right) \tag{34}$$

When the current corresponds to complete H_2 recovery:

$$\frac{P_C}{P_A} \exp\left(\frac{-2\mathfrak{F}V}{RT}\right) = 0 \qquad \therefore V \to \infty \tag{35}$$

Hence, as equations (30) to (35) prove, the relationship between energy and recovery is asymptotic in nature, with the expression going to infinity as recovery goes to 100%.

Figure 26 showcases an entirely different calculation that demonstrates how the unit cost of each additional energy input becomes greater than the unit cost of each additional H_2 unit recovered.

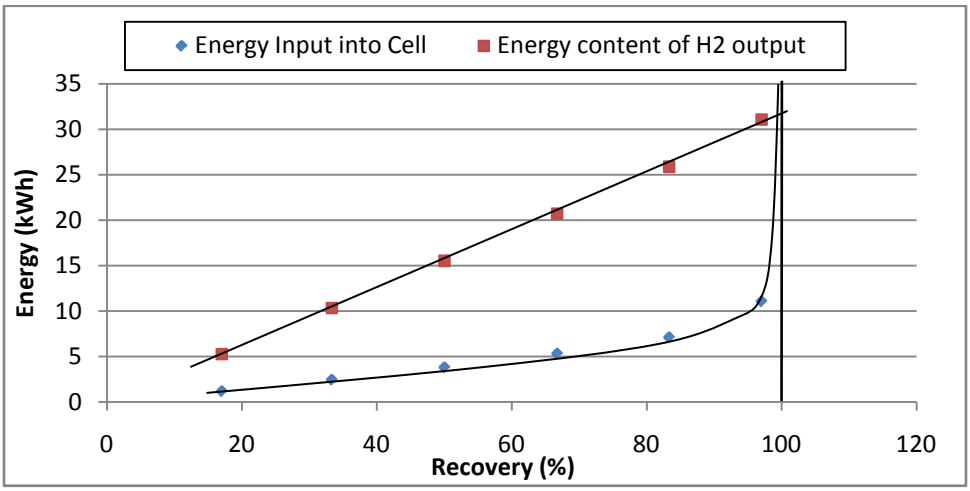

Figure 26: *By the very asymptotic nature of the energy efficiency function (recovery/power), the insistence on high yield means that, eventually, the unit cost of each energy input into the cell will become greater than the unit energy content of each H_2 output from the pumping operation. At this point, it is economically indefensible to continue the pumping operation.*

Part V – A Discussion of Experimental Limitations

The Arbin performed superbly as a DAQ system, but the inclusion of a temperature DAQ system that would record the temperature of the fuel cell, the humidifier, and the heating tape tracing the gas lines would ensure that close attention is paid to the membrane's condition in terms of its humidity, and would help determine whether the cell's degradation in performance is related in any way to the excess or dearth of water in the cell itself – since both affect performance to a great extent.

The GDTs readings were perhaps not as accurate as they could have been, primarily due to the fact that the anode GDTs are graduated only at 5v% intervals, and the cathode GDTs were easily influenced by brief exposures to air. Also, the GDTs could

only determine the v% of CO_2 present in the outlet streams. It would have been interesting to see whether CO was present at the anode outlet, given our claim that CO poisoning was insignificant at the conditions investigated. The best way to correct this would be to employ a gas chromatograph (GC) with a thermal conductivity detector (TCD) to determine the composition of anode and cathode outlets to a higher accuracy.

Perhaps the biggest limitation is the relatively short span of the runs themselves. Running the 3:1 H_2:CO_2 mixture for hundreds of hours as opposed to 5-10 hours may confirm significant performance degradation over time as a direct result of CO poisoning.

Part VI – Conclusions

We set out to determine how CO_2 affects the performance of an electrochemical pump at different temperatures and concentrations. Our results show that temperature has a small effect on a 1-cell hydrogen pump in terms of increasing power requirements. If the RWGS mechanism is responsible for cell poisoning, this explains our observations. In terms of η_{H_2}, η_{cell}, and η_{sep}, temperature has no effect, as expected. Moreover, temperature has no effect on the level of CO_2 diffusion from the anode to the cathode.

Feed composition, on the other hand, has a significant effect on cell performance. As the H_2 concentration decreases in the feed, the power requirements increase exponentially. Furthermore, the behavior of voltage over time becomes more erratic as the H_2 concentration decreases. This behavior is not permanent; membrane relaxation alone can alleviate the degradation in performance without any need for current pulsing or an air bleed, which suggests that CO poisoning is not as great as literature studies suggest – at least at low currents. It is the dilution of H_2 in the feed, and the covering of adsorption sites at the anode catalytic interface by CO_2 molecules that forces the cell's

potential to rise: in other words, it is a question of getting the H_2 molecules to the three-way interface at low H_2 concentrations (mass transfer limitations) that is the culprit.

Simulations of both a 4-cell and a 6-cell electrochemical pumps were performed, which generated H_2 yields of 67% and >99%, respectively. The cell efficiencies of the individual cells in the two stacks were between 93% and 96%. As the CO_2 concentration at the anode increased, the CO_2 concentration at the cathode increased, suggesting that the driving force for the diffusion responsible for CO_2 transport from the anode to cathode increases with the CO_2 concentration. Despite these increases at the cathode, the CO2 concentration was 1500ppm in the 4-cell stack and 2500ppm in the 6-cell stack, and the separation efficiencies were 99.85% in the former case and 99.72% in the latter.

The combination of high yield, high separation efficiency, low current, and low power requirement makes this setup a viable solution to H_2 separation from a reformate mix. If CO formation is suppressed in refining steps preceding the separation itself, or if the CO is catalytically converted to CO_2 by passing the mix through a fixed catalytic bed, H_2 pumping can definitely be considered a solution to the issue of distributed (or localized) H_2 purification prior to H_2 use in FCVs or other fuel cell stations.

Part VI – Future Work

Future experiments should focus on determining whether the efficiency figures seen in this study change if pumping schedules run for longer periods of time. Also, the presence of CO needs to be verified or disproved through gas chromatography to determine which poisoning mechanism governs CO_2 behavior at these conditions: is it CO formation through the RWGS or reduction reactions, or is the dilution factor

dominant, as suggested in this paper. Finally, although we know the operating costs of this setup are bound to be low, an economic analysis needs to be carried out to compare the *capital* costs involved in medium-scale PSA and cryogenic distillation as opposed to electrochemical pumping.

References

[1] Energy Information Administration. Forecasts and Analysis of Energy Data: U.S. Data Projections. http://www.eia.doe.gov/oiaf/forecasting.html. Accessed March 2009. Report #:DOE/EIA-0383(2009)

[2] U.S. Department of Energy. Hydrogen Program. http://www.hydrogen.energy.gov/about.html. Accessed February 2009.

[3] DOT. Hydrogen Portal. http://hydrogen.dot.gov/program/. Accessed February 2009.

[4] International Partnership for the Hydrogen Economy. About IPHE. http://www.iphe.net/about.html. Accessed February 2009.

[5] NY State Energy Research and Development Authority. Hydrogen Production – Steam Methane Reforming (SMR). http://www.getenergysmart.org/Files/HydrogenEducation/6HydrogenProductionSteamMethaneReforming.pdf. Accessed March 2009.

[6] International Energy Agency. World Energy Outlook 2008. http://www.worldenergyoutlook.org/docs/weo2008/WEO2008_es_english.pdf. Accessed February 2009.

[7] The Association for the Study of Peak Oil and Gas "ASPO". Newsletter No. 92 – August 2008. http://www.aspo-ireland.org/contentFiles/newsletterPDFs/newsletter92_200808.pdf. Accessed February 2009. pp. 2.

[8] Financial Times. World Bank cuts China growth Forecast. March 18, 2009. http://www.ft.com/cms/s/0/7c3dcc82-137c-11de-9e32-0000779fd2ac.html. Accessed March 2009.

[9] BusinessWeek. What's Wrong with 6% GDP Growth for India. March 11, 2009. http://www.businessweek.com/globalbiz/content/mar2009/gb20090311_895802.htm. Accessed March 2009.

[10] Simmons, Matthew R. "Twilight in the Desert: The Risk of Peak Oil." Minnesota House of State Representatives. Minnesota, St. Paul. 4 Feb. 2008.

[11] Energy Information Administration. Forecasts and Analysis of Energy Data: U.S. Data Projections.

[12] "Marketplace: Oil demand could soon outstrip supply." Marketplace from American Public Media. http://marketplace.publicradio.org/display/web/2008/01/25/out_of_oil_within_seven_years/. Accessed March 2009.

[13] Hogarth, Warren H.J.; Benziger, Jay B.; Operation of polymer electrolyte membrane fuel cells with dry feeds: Design and operating strategies. *Journal of Power Sources*. **2006**, 159, 968-978.

[14] Perry K.A.; Glenn A.E.; Benicewicz B.C.; Electrochemical hydrogen pumping using a high-temperature polybenzimidazole (PBI) membrane. *Journal of Power Sources*. **2008**, 177, 478-484.

[15] Gardner C.L., and Ternan, M. Electrochemical separation of hydrogen from reformate using PEM fuel cell technology. *Journal of Power Sources.* **2007**, 171, 835-841.

[16] Hyperphysics. Electrolysis of Water. http://hyperphysics.phy-astr.gsu.edu/hbase/thermo/electrol.html. Accessed March 2009.

[17] Science Daily. Solar Cell Directly Splits Water To Produce Recoverable Hydrogen. 19 February, 2008. http://www.sciencedaily.com/releases/2008/02/080217170412.htm. Accessed January 2009.

[18] U.S. Department of Energy. Hydrogen Production. http://www1.eere.energy.gov/hydrogenandfuelcells/production/natural_gas.html. Accessed February 2009.

[19] Esselink B.V. Process Description. http://www.esselinkbv.com/descr.html. Accessed March 2009.

[20] Universal Industrial Gases Inc. Overview of Cryogenic Air Separation and Liquefier Systems. http://www.uigi.com/cryodist.html. Accessed January 2009.

[21] Sherman, J.D. Synthetic zeolites and other microporous oxide molecular sieves. *Proceedings of the National Academy of Sciences*. **1999**, 96, 3471-3478.
[22] Hydrogen Production and Storage – R&D Priorities and Gaps. IEA Hydrogen Implementing Agreement. **2006**.
[23] Rohland, B.; Eberle, K.; Ströbel, R.; Scholta, J.; Garche, J.; Electrochemical hydrogen compressor, *Electrochimica Acta*, **1998**, 43, 3841-3846.
[24] Barbir, F.; Görgün, H.; Electrochemical hydrogen pump for recirculation of hydrogen in a fuel cell stack, *Journal of Applied Electrochemistry*, **2007**, 37, 359-365.
[25] Sedlak, J.M.; Austin, J.F.; LaContin A.B.; *International Journal of Hydrogen Energy*, **1981**.
[26] Yang, C.; Costamagna, P.; Srinivasan, S.; Benziger, J.; Bocarsly, A.B.; Approaches and technical challenges to high temperature operation of proton exchange membrane fuel cells, *Journal of Power Sources*, **2001**, 103, 1-9.
[27] Casati, C.; Longhi, P.; Zanderighi, L.; Bianchi, F.; Some fundamental aspects in electrochemical hydrogen purification/compression, *Journal of Power Sources*, **2008**, 180, 103-113.
[28] Tingelöf, T.; Hedström, L.; Holmström, N.; Alvfors, P.; Lindbergh, G.; The influence of CO2, CO and air bleed on the current distribution of polymer electrolyte fuel cell. *International Journal of Hydrogen Energy*, **2008**, 33, 2064-2072.
[29] U.S. Department of Energy. Carbon Sequestration R&D. http://fossil.energy.gov/programs/sequestration/overview.html . Accessed April 2009.
[30] Ren, X.; Gottesfeld, S.; Electro-osmotic Drag of Water in Poly(perfluorosulfonic acid) Membranes, *Journal of the Electrochemical Society*, **2001**, 148, A87-A93.
[31] de Bruijn, F.A.; Papageorgopoulous, D.C.; Sitters, E.F.; Janssen, G.J.M.; The influence of carbon dioxide on PEM fuel cell anodes, *Journal of Power Sources*, **2002**, 110, 117-124.
[32] Ralph, T.R.; Hogarth, M.P.; Catalysis for low temperature fuel cells, *Platinum Metals Review*, **2002**, 46(3), 117-135.
[33] Mench, M.; *Fuel Cell Engines*; John Wiley & Sons: Hoboken, NJ, **2008**. pp. 466.
[34] U.S. Department of Energy. Hydrogen from Coal Program: Research, Development, and Demonstration Plan for the Period 2008 through 2016. External Draft. September 2008.
[35] Johnson, Michael C. "The Cost of Hydrogen Separation Systems." E-mail to the author. 6 May 2009.
[36] "Hydrogen Management with PSA and Recovery Equipment." UOP. 08 May 2009 <http://www.uop.com/refining/1100.html>.
[37] Choi, Yongtaek, and Harvey G. Stenger. "Water gas shift reaction kinetics and reactor modeling for fuel cell grade hydrogen." Journal of Power Sources 124 (2003): 432-39.